# Numerical analysis of water flow characteristics after inrushing from the tunnel floor in process of karst tunnel excavation

S.C. Li [*], J. Wu [a], Z.H. Xu [b], L.P. Li [c], X. Huang [d], Y.G. Xue [e] and Z.C. Wang [f]

*Geotechnical and Structural Engineering Research Center,
Shandong University, Ji'nan 250061, Shandong, China*

**Abstract.**    In order to investigate water flow characteristics after inrushing in process of karst tunnel excavation, numerical simulations for five case studies of water inrush from the tunnel floor are carried out by using the FLUENT software on the background of Qiyueshan high risk karst tunnel. Firstly, the velocity-distance curves and pressure-distance curves are drawn by selecting a series of probing lines in a plane. Then, the variation characteristics of velocity and pressure are analyzed and the respective optimized escape routes are made. Finally, water flow characteristics after inrushing from the tunnel floor are discussed and summarized by comparing case studies under the conditions of different water-inrush positions and excavation situations. The results show that: (1) Tunnel constructors should first move to the tunnel side wall and then escape quickly when water inrush happens. (2) Tunnel constructors must not stay at the intersection area of the cross passage and tunnels when escaping. (3) When water inrush from floor happens in the left tunnel, if tunnel constructors meet the cross passage during escaping, they should pass through it rapidly, turn to the right tunnel and run to the entrance. (4) When water inrush from floor happens in the left tunnel, if there is not enough time to escape, tunnel constructors can run to the trolley and other equipment in the vicinity of the right tunnel working face. In addition, some rescuing equipment can be set up at the high location of the cross passage. (5) When water inrush from floor happens in the cross passage, tunnel constructors should move to the tunnel side wall quickly, turn to the tunnel without water inrush and run to the entrance. (6) When water inrush from floor happens in the cross passage, if there is not enough time to escape, tunnel constructors can run to the trolley and other equipment near by the left or the right tunnel working face. The results are of important practical significance and engineering value to ensure the safety of tunnel construction.

**Keywords:**    water inrush; velocity; pressure; flow characteristic; optimized escape routes; karst tunnel

## 1. Introduction

Tunnel project is one of the main forms of underground engineering (Do *et al.* 2014, Fahimifar

*Corresponding author, Ph.D., Professor, E-mail: lishucai@sdu.edu.cn
[a] Ph.D. Student, E-mail: wujing9516@163.com
[b] Ph.D., Lecturer, E-mail: zhenhao_xu@sdu.edu.cn
[c] Ph.D., Associate Professor, E-mail: yuliyangfan@163.com
[d] Ph.D. Student, E-mail: hx19891018@yeah.net
[e] Ph.D., Professor, E-mail: xieagle@sdu.edu.cn
[f] Ph.D., Associate Professor, E-mail: wanz@sdu.edu.cn

*et al.* 2015). At present, the largest number of tunnels in the world is constructed in China, and its speed of development is also the fastest. With the accelerating process of China's infrastructure construction, there will be more deep and long tunnels in transportation, water conservancy and hydropower, mineral resources exploitation and other fields (Yang and Yan 2015). These tunnel projects generally show notable features with large depth, great length and complex hydrogeological conditions. Moreover, the geological exploration work of pre-construction is hard to identify hydrogeological condition along the tunnel clearly. There will lead to many geological disasters in process of tunnel excavation, such as rock burst, collapse, gas outburst, water inrush and mud inrush, etc. (Zarei *et al.* 2012, Xu *et al.* 2014, Li *et al.* 2014). Among them, water inrush is one of the main geological disasters during the construction of karst tunnels (Zhang 2005, Li *et al.* 2009b, Liu *et al.* 2010, Wang and Wang 2011, Wu *et al.* 2011a, Wang *et al.* 2012, Zhou *et al.* 2015). The occurrence frequency and death toll caused by water inrush are both on the top levels in serious tunnel accidents at home and abroad (Qian *et al.* 2002, Lei *et al.* 2003, Ivars 2006, Li *et al.* 2007, Liu *et al.* 2011, Qian 2012). Water inrush results from the joint effects of human activity, geologic activity and other factors, and its major hazards are as follows (Li and Zhang 1995, Islam and Islam 2005, Kong and Chen 2006, Kong *et al.* 2007, Shang *et al.* 2007, Li *et al.* 2010b).

Water inrush can cause great casualties and huge economic losses. Water inrush usually accompanies gushing mud, gushing sand and even rolling stones, which leads to tunnel flooding, machineries destruction, construction interruption and project delay. Water-inrush disasters occurred in the high-pressure and water-rich regions often have strong destructiveness, which can easily cause severe personnel casualty, and have great hazards to the safety of tunnel construction. According to the statistics, during the construction of Chengdu-Kunming railway, Datong-Qinhuangdao railway and Beijing-Guangzhou railway, the downtime caused by hydrological and geological problems accounts for 1/3~1/4 of the total construction period. For Chongqing-Huaihua Railway (Yuanliangshan tunnel), it appears 71 times severe water inrush. The maximum water inflow is 72,000 $m^3$/h, and 9 tunnel constructors died. For Yichang-Wanzhou Railway (Yesanguan tunnel), a large water-inrush accident occurs in August 2007. The water inflow is 151,000 $m^3$ within a half hour, and 10 tunnel constructors died. The project duration is delayed for six months. For Shanghai-Chengdu Expressway (Longtan tunnel), it appears 2 times severe water inrush. The water inflow is over 9,000 $m^3$. The project duration is delayed for more than one year (Fig. 1(a)). At abroad, Japan's Seikan Tunnel encounters 4 times water inrush of 115,200 $m^3$/d, and a total of 34 tunnel constructors died. The accident is controlled after more than five months. The project duration is delayed for more than ten years. In addition, there are many other water-inrush disasters, such as GD-3 hydroelectric station (Diversion tunnel) in Ethiopia, Dul Hasti hydroelectric station (Diversion tunnel) in India, Frasnadello tunnel and Antea tunnel in Italy, etc. They also suffer different levels of water-inrush disasters. Obviously, water-inrush disasters have brought huge economic losses and safety issues for tunnel construction, which has become a major issue facing the tunnel engineering.

In addition, water inrush can induce secondary geological disasters and environmental problems. Water inrush causes the sudden change of effective stress and the fluctuation of hydrodynamic pressure within a short time in overlying strata, which induces surface subsidence, landslide and other secondary geological disasters. It not only brings many problems for tunnel construction, but also influences the production and life of local residents greatly (Fig. 1(b)). Water inrush can break the balance of groundwater systems, and result in the relationship between underground seepage field and groundwater recharge-discharge changing drastically, and cause decline of the water table, exhaustion of groundwater resources, water pollution and other
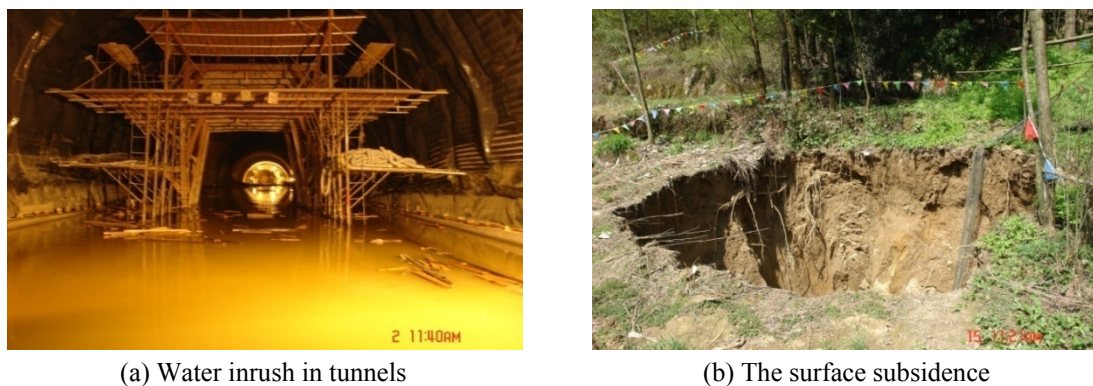
(a) Water inrush in tunnels



(b) The surface subsidence

Fig. 1 Water inrush in Qiyueshan tunnel of Hurongxi Highway

problems. Moreover, the decline of the water table can cause the destruction and death of surface vegetation. Overall, water inrush can bring a series of ecological environmental problems, which seriously affects the sustainable development of local society, economy and environment.

As seen above, water-inrush disasters have brought huge economic losses, great casualties and negative social impacts (Huang *et al*. 2010, Cho *et al*. 2013, Li *et al*. 2013). They also cause irreparable damage to the earth's surface, water resource and ecological environment in tunnel zone (Shi and Singh 2001, Zhang and Peng 2005, Wu *et al*. 2008, Li *et al*. 2015a). Therefore, the investigation for prevention and treatment of water-inrush, and water flow characteristics after inrushing should be carried out. The investigation is the urgent requirement for guaranteeing the safety of tunnel construction, and it has important engineering value and practical significance.

At present, people focus on two aspects researches in the field of prevention and treatment of water-inrush (Wang *et al*. 2003, 2004, Liao *et al*. 2006, Zhang and Fu 2007, Zhang *et al*. 2009, Shi and Xu 2010, Chen *et al*. 2014, Li *et al*. 2015b). Firstly, in order to apply theory guide engineering practice, the development rules of karst and mechanism of water-inrush are studied, and the growth rules of karst water-inrush are analyzed. Secondly, on-the-spot applicable detection means and water-inrush control measures are investigated. The effective early warning mechanisms of karst water-inrush and control technique systems are established. Now the main research results are as follows.

Golob *et al*. (1998) presented a new approach to forecast water inflow based on neural networks. The efficacy of the proposed method was tested for a practical case, and some results were concluded. Marinelli and Niccoli (2000) presented steady-state analytical solutions for estimating the ground water inflow rate in a mine pit. Di *et al*. (2005) put forward integrated geophysical exploration technique. It was conducted with controlled source audio magnetic telluric (CSAMT) method which was the main exploration method, VLF method, IP and TEM methods. The technique was applied to the deep-lying tunnels with a length of 20 km in west route of South-to-North Water Transfer Project. Qu *et al*. (2006) proposed a synthetic geological prediction method based on system theory, and the method involved three geological prediction techniques, i.e., ground geologic survey, GPR and TSP. The synthetic prediction method was discussed in detail, and the realization process was put forward. The proposed method was applied to the advance geological forecast of Guangrenling tunnel. Li *et al*. (2007) first introduced the recent development of the forecast and the integration system of the forecast about the karst-fractured groundwater and the defective geological conditions in detail. The key issues of the karst-fractured

groundwater and the defective geological conditions in prediction were derived. The methods of forecasting defective geological conditions and karst-fractured groundwater with high pressure and large flow were summarized. Wang and Lu (2007) proposed a semi-analytical approach for analyzing the tunnel water inflow. The approach was developed by using the classical ground water theory. Wang *et al*. (2007) came up with a complete set of geological forecasting techniques including the macro forecast, the long-term prediction, the short-term prediction and the forewarning methods of the disasters based on the theory of geomechanics. According to the practical test of the prediction in Xiamen subsea tunnel, the accuracy of the prediction could meet the requirements of the construction standards. Li *et al*. (2008) proposed four-color warning method of tunnel geological disasters. The corresponding contingency plans were developed based on comprehensive geological prediction. The four-color warning method and comprehensive geological prediction method had been applied successfully for many projects to avoid casualties and serious economic losses, which had guiding significance to similar projects. Zhu *et al*. (2008) developed a numerical model of the key strata. It included structural characteristics and mechanical properties of the floor rock at the working face of a particular coal mine. The model was used to predict failure modes and help establish rules for safe mining above the aquifer. Due to the activation of collapse columns with full water-filling and border water-filling, Li *et al*. (2009a) simulated the water inrush process by using RFPA2D code. The numerical simulation duplicated the whole process of forming the macro water and conducting channels from water-filling collapse columns. The purpose was to study the failure pattern of collapse columns and the mechanism of water inrush from coal seam floor. Li *et al*. (2010a) studied the mechanism of water-rock interaction in karst tunnels by using theories of karst geology, engineering hydraulics and fracture mechanics. The effects of such mechanism on water and mud inrush during the construction of karst tunnels were explored, and the mechanical mechanism of water inrush process was analyzed. Zhu and Wei (2011) used a model to simulate the mining-induced groundwater inrush, at the same time, the effects of faults and karst collapse columns were considered in the numerical simulation. Some suggestive conclusions for preventing water inrush and optimizing underground mining operations were drawn. Huang *et al*. (2012) built a stress-seepage coupling model for rock based on the fluid-solid coupling theory, then they combined with an example of water-inrush caused by fault, studied the water-inrush mechanism by using the numerical software COMSOL, analyzed the change rules of shear stress, vertical stress, plastic area and water pressure with a fault, and estimated the water-inrush risk at the different distances between the working face and the fault. Shi *et al*. (2014) indicated that both water inrush coefficient and water abundance in aquifers should be taken into consideration when evaluating the danger of water inrush from coal seam floor. They built a prediction model of safe-mining evaluation grade by using the support vector machine, and the results showed that this model had high classification accuracy. In addition, the publications (Li *et al*. 1996, Yin and Wu 2004, Hu *et al*. 2008, Jin *et al*. 2009, Ma *et al*. 2010, Xu *et al*. 2011, Wu *et al*. 2011b, Meng *et al*. 2012, Yao *et al*. 2012, Ling *et al*. 2015) also considered the prevention and treatment of water inrush.

However, conventional investigation often focuses on how to probe and prevent karst water in domestic and foreign studies. The investigation for water flow characteristics after inrushing is often ignored. Relevant research is also seldom related to the specific work of formulating optimized escape routes. In the present study, Qiyueshan high risk karst tunnels are taken as studying background. Five case studies of water inrush from the tunnel floor are simulated during the double-line tunnel excavation by using the FLUENT software. The corresponding velocity contour, pressure contour, velocity vector and velocity streamline are obtained. In order to show

the variation of velocity and pressure in the tunnels more clearly, a series of probing lines are selected in a plane, and the variation rules of velocity and pressure along with distance are analyzed, which purpose is to obtain the optimized escape routes. Finally, combined with this study, the water flow characteristics after inrushing from the tunnel floor are discussed and summarized by comparing the case studies under the conditions of different water-inrush positions and excavation situations, which has important guiding significance for making scientific and rational escape routes and rescue routes.

## 2. Numerical simulation models

Because the velocity of water affected by the tunnel section is little, so the tunnel section is simplified, i.e., the original three concentric circles are simplified to straight wall arch.

With the background of Qiyueshan tunnels, the 100 meters behind the working face are selected. The finite element model is built in ANSYS Workbench. The specific model dimensions
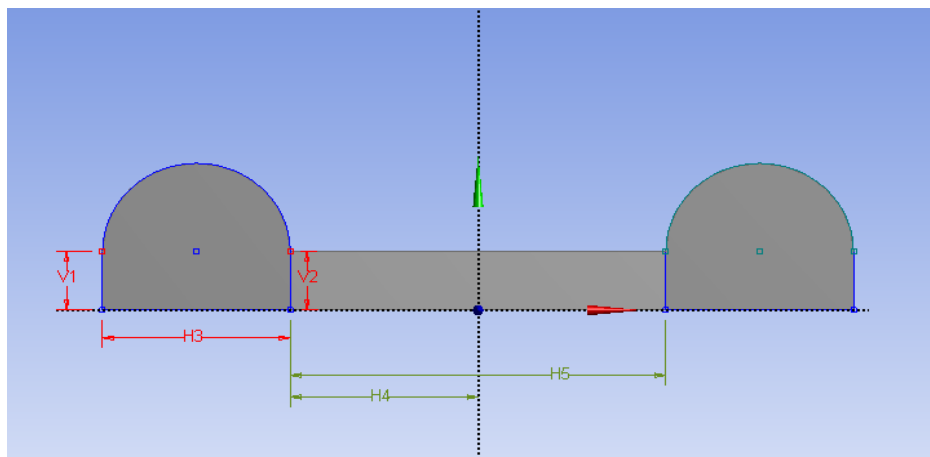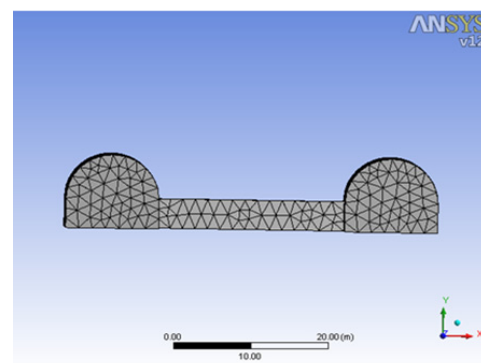


Fig. 2 The model dimensions
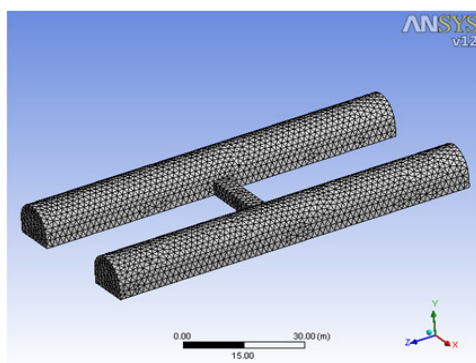


(a)                                                    (b)

Fig. 3 The finite element models

are shown in Fig. 2. Wherein, V1 = V2 = 4 m, H3 = 12 m, H4 = 12 m, H5 = 24 m. Tunnel cross-sectional area S = 104.52 m$^2$, the total height of the tunnels Y = 10 m (the height of the upper part is 6 m, and the height of the lower part is 4 m), the total length of the tunnels Z = 100 m, the distance of axle line between the left tunnel and the right tunnel X = 36 m, the width of the cross passage Z1 = 4 m, the height of the cross passage Y1 = 4 m, the length of the cross passage X1 = 24 m, the distance between the axle line of the cross passage and the working face Z0 = 50 m. The finite element models are shown in Fig. 3.

## 3. Parameters and boundary conditions

Calculation parameters are selected as follows. The direction of gravity acceleration is Y-axis negative direction, the value is 9.8 m/s$^2$. The basic physical model adopts the standard k-e turbulence model. Fluid material chooses 20°C liquid water, and its physical parameters are as follows: Density is 998.2 kg/m$^3$, specific heat capacity is 4182 j/kg·k, thermal conductivity is 0.6 w/m·k, viscosity is 100.3×10$^{-5}$ pa·s. The water is incompressible adiabatic fluid. The steady-state analysis techniques are adopted in the process of calculation.

There are velocity inlet boundary condition, the pressure inlet boundary condition, the quality inlet boundary condition, the pressure outlet boundary condition, etc. in fluid simulation of FLUENT. The velocity is assumed 2 m/s in this simulation. Because the water cannot pass through the tunnel side wall, so the velocity at this location is 0 m/s. The water is mainly gushed from the tunnel entrance, so the pressure at this location is 0 Pa. Therefore, the boundary conditions are set as the velocity inlet boundary condition and pressure outlet boundary condition. In addition, the calculation analysis adopts turbulence models. The fluid is incompressible, so the variation of kinetic energy and viscous dissipation can be ignored.

## 4. Case studies

Five common cases of water inrush from floor are simulated during the tunnel excavation. The first case, water inrush from floor occurs in the bottom of the left tunnel working face. The area of water inrush is 48 m$^2$ (X × Z = 12 m × 4 m) and the velocity is 2 m/s. The left and the right tunnel entrances are pressure outlet boundaries. The second case, water inrush from floor occurs in the middle position of the cross passage. The area of water inrush is 48 m$^2$ (X × Z = 12 m × 4 m) and the velocity is 2 m/s. The left and the right tunnel entrances are pressure outlet boundaries. The third case, water inrush from floor occurs in the bottom of the left tunnel working face (away from the left tunnel entrance). The area of water inrush is 48 m$^2$ (X × Z = 12 m × 4 m) and the velocity is 2 m/s. The right tunnel entrance is a pressure outlet boundary. The forth case, water inrush from floor occurs in the middle position of the cross passage. The area of water inrush is 48 m$^2$ (X × Z = 12 m × 4 m) and the velocity is 2 m/s. The right tunnel is a pressure outlet boundary. The fifth case, water inrush from floor occurs in the bottom of the left tunnel working face (close to the left tunnel entrance). The area of water inrush is 48 m$^2$ (X × Z = 12 m × 4 m) and the velocity is 2 m/s. The right tunnel entrance is a pressure outlet boundary.

### 4.1 Case study 1

During the double-line tunnel excavation, water inrush from floor occurs in the bottom of the left tunnel working face, i.e., the floor below the left tunnel working face is the inlet of water

inrush (velocity, 2 m/s), and the left and right tunnel entrances are the outlets of water inrush (pressure, 0 Pa). The scope of water inrush along the length direction of the left tunnel (Z-direction) is 4 m, and the width direction of the left tunnel (X-direction) is 12 m. The total area of water inrush is 48 m$^2$. As shown in Fig. 4, A is the water inrush position.
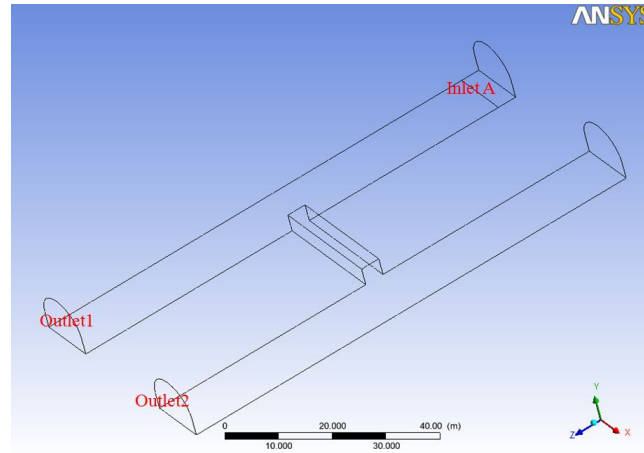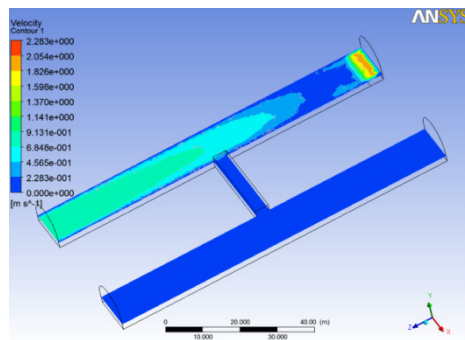


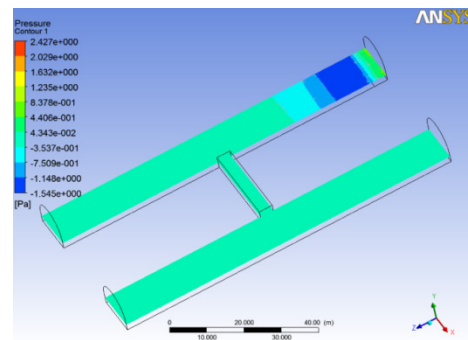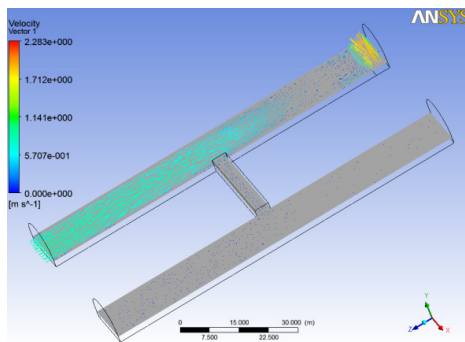Fig. 4 The water inrush position in the left tunnel (Case 1)



(a) Velocity contour



(b) Pressure contour



(c) Velocity vector



(d) Velocity streamline

Fig. 5 Y = 2 section
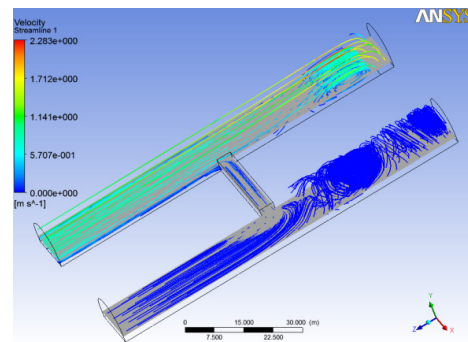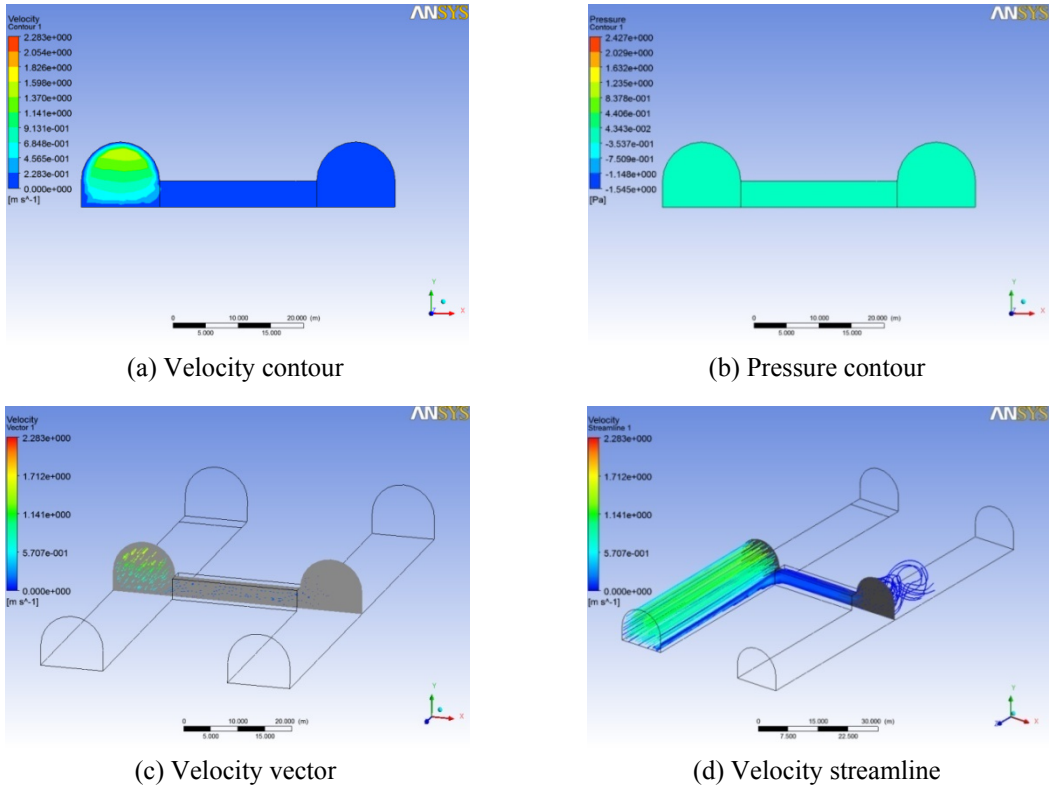
(a) Velocity contour



(b) Pressure contour



(c) Velocity vector



(d) Velocity streamline

Fig. 6 Z = 50 section

### 4.1.1 Simulated results

Y = 2 section and Z = 50 section are selected as examples. The calculation results are shown in Figs. 5 and 6.

### 4.1.2 Analysis

In order to show the changes of velocity and pressure in the tunnels more clearly, a series of probing lines are selected. The details of the probing lines are shown in Table 1, and the corresponding figures are shown in Fig. 7. The probing lines are researched and analyzed.
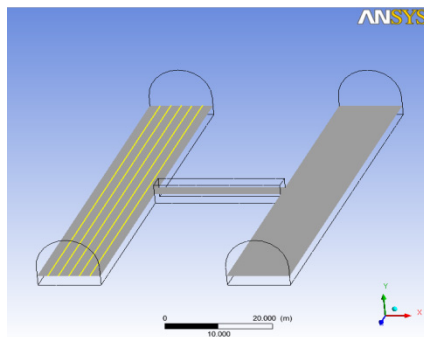
Table 1 The details of the probing lines

| The section | The location | The selected probing lines | The selected points | The figure |
|---|---|---|---|---|
| | | X = -14, Y = 2, Z = 0~100 | 20 | |
| | | X = -16, Y = 2, Z = 0~100 | 20 | |
| Y = 2 | The left tunnel | X = -18, Y = 2, Z = 0~100 | 20 | Fig. 7(a) |
| | | X = -20, Y = 2, Z = 0~100 | 20 | |
| | | X = -22, Y = 2, Z = 0~100 | 20 | |

Table 1 Continued

| The section | The location | The selected probing lines | The selected points | The figure |
|---|---|---|---|---|
| Y = 2 | The cross passage | Y = 2, Z = 48.4, X = -12~12 | 20 | Fig. 7(b) |
| | | Y = 2, Z = 49.2, X = -12~12 | 20 | |
| | | Y = 2, Z = 50.0, X = -12~12 | 20 | |
| | | Y = 2, Z = 50.8, X = -12~12 | 20 | |
| | | Y = 2, Z = 51.6, X = -12~12 | 20 | |
| Y = 2 | The right tunnel | X = 14, Y = 2, Z = 0~100 | 20 | Fig. 7(c) |
| | | X = 16, Y = 2, Z = 0~100 | 20 | |
| | | X = 18, Y = 2, Z = 0~100 | 20 | |
| | | X = 20, Y = 2, Z = 0~100 | 20 | |
| | | X = 22, Y = 2, Z = 0~100 | 20 | |
| X = -18 | The left tunnel | X = -18, Y = 0.4, Z = 0~50 | 10 | |
| | | X = -18, Y = 1.2, Z = 0~50 | 10 | |
| | | X = -18, Y = 2.0, Z = 0~50 | 10 | |
| | | X = -18, Y = 2.8, Z = 0~50 | 10 | |
| | | X = -18, Y = 3.6, Z = 0~50 | 10 | |
| Z = 50 | The cross passage | Y = 0.4, Z = 50, X = -18~18 | 10 | Fig. 7(d) |
| | | Y = 1.2, Z = 50, X = -18~18 | 10 | |
| | | Y = 2.0, Z = 50, X = -18~18 | 10 | |
| | | Y = 2.8, Z = 50, X = -18~18 | 10 | |
| | | Y = 3.6, Z = 50, X = -18~18 | 10 | |
| X = 18 | The right tunnel | X = 18, Y = 0.4, Z = 50~100 | 10 | |
| | | X = 18, Y = 1.2, Z = 50~100 | 10 | |
| | | X = 18, Y = 2.0, Z = 50~100 | 10 | |
| | | X = 18, Y = 2.8, Z = 50~100 | 10 | |
| | | X = 18, Y = 3.6, Z = 50~100 | 10 | |



(a)                    (b)

Fig. 7 The location of the probing lines

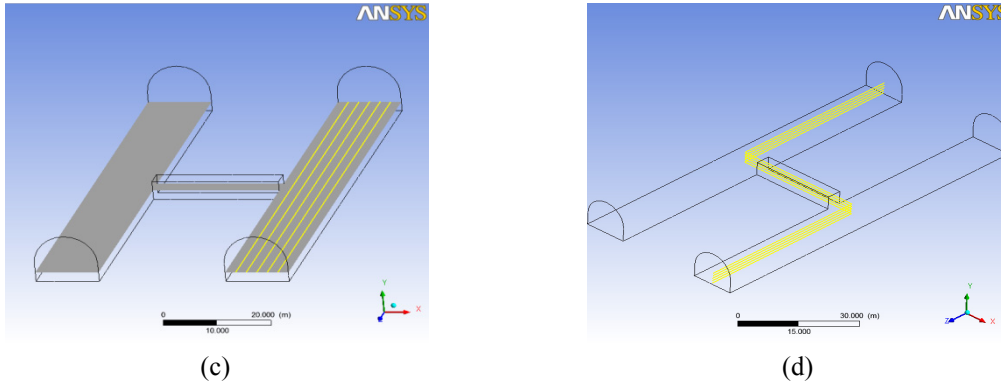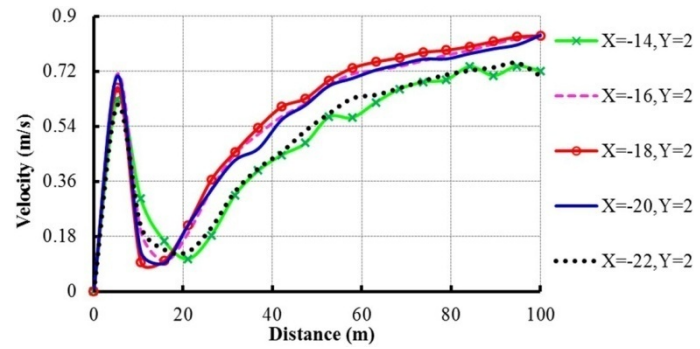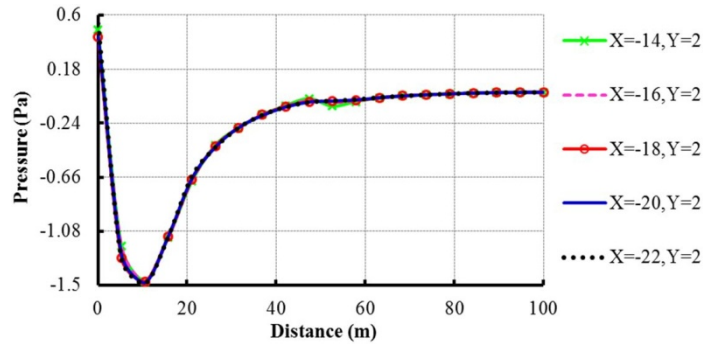(c)                                                  (d)

Fig. 7 Continued



(a) Velocity curves



(b) Pressure curves

Fig. 8 The velocity and pressure curves of the left tunnel

(1)  As for the five probing lines in the left tunnel (Fig. 7(a)), their velocity curves and pressure curves are shown in Fig. 8.

It can be obtained from Fig. 8:

(i)  Fig. 8(a) shows that, when X = -14, Y = 2, the variation range of velocity is from 0 m/s to 0.722 m/s. When X = -16, Y = 2, the variation range of velocity is from 0 m/s to 0.837 m/s.

When X = -18, Y = 2, the variation range of velocity is from 0 m/s to 0.846 m/s. When X = -20, Y = 2, the variation range of velocity is from 0 m/s to 0.838 m/s. When X = -22, Y = 2, the variation range of velocity is from 0 m/s to 0.705 m/s.

(ii)  Overall, the variation range of velocity in the left tunnel is from 0 m/s to 0.846 m/s. The velocity changes greatly, and it is high speed-based. The velocity near by the water inrush position (A) is large, and then it decreases rapidly along with the increase of the distance. About 15 m~20 m from the working face, the value is smaller, then, the velocity increases gradually, and it reaches its maximum value at the left tunnel entrance (Outlet 1). In addition, it also can be concluded, the velocity in the center of the section is the maximum, and then it decreases gradually toward both sides of the section, i.e., the velocity is the maximum when X = -18, while the velocity is the minimum when X = -14 or X = -22.

(iii) Fig. 8(b) shows that, when X = -14, Y = 2, the variation range of pressure is from -1.47 Pa to 0.485 Pa. When X = -16, Y = 2, the variation range of pressure is from -1.47 Pa to 0.449 Pa. When X = -18, Y = 2, the variation range of pressure is from -1.47 Pa to 0.432 Pa. When X = -20, Y = 2, the variation range of pressure is from -1.48 Pa to 0.464 Pa. When X = -22, Y = 2, the variation range of pressure is from -1.49 Pa to 0.534 Pa.

(iv)  In general, the pressure in the position of the working face is the maximum, and then it decreases rapidly along with the increase of the distance. About 10 m from the working face, the pressure reaches its maximum negative value, and then it increases gradually. The pressure becomes 0 Pa at the location of the left tunnel entrance (Outlet 1). In addition, the pressure curves of five probing lines coincide well, which shows that, in the width direction of the left tunnel (X-direction), the pressure values along the length direction of the left tunnel (Z-direction) are fixed.

(2)  As for the five probing lines in the cross passage (Fig. 7(b)), their velocity curves and pressure curves are shown in Fig. 9.

It can be obtained from Fig. 9:

(i)  Fig. 9(a) shows that, when Y = 2, Z = 48.4, the variation range of velocity is from 0.033 m/s to 0.12 m/s. When Y = 2, Z = 49.2, the variation range of velocity is from 0.094 m/s to 0.192 m/s. When Y = 2, Z = 50, the variation range of velocity is from 0.13 m/s to 0.253 m/s. When Y = 2, Z = 50.8, the variation range of velocity is from 0.087 m/s to 0.202 m/s. When Y = 2, Z = 51.6, the variation range of velocity is from 0.03 m/s to 0.09 m/s. The maximum velocity appears at the starting point of the center line, i.e., X = -12, Y = 2, Z = 50.

(ii)  In the process of flowing from the left tunnel to the cross passage, the velocity reduces obviously. The variation range of velocity in the cross passage is from 0.03 m/s to 0.253 m/s, and the velocity is low speed-based. The velocity in the center of the section is the maximum, and then it decreases gradually toward both sides of the section, i.e., the velocity is the maximum when Z = 50, while the velocity is the minimum when Z = 51.6. Overall, as the distance (X) increases, the velocity gets smaller and smaller.

(iii)  Fig. 9(b) shows that, when Y = 2, Z = 48.4, the variation range of pressure is from -0.023 Pa to -0.013 Pa. When Y = 2, Z = 49.2, the variation range of pressure is from -0.025 Pa to -0.013 Pa. When Y = 2, Z = 50, the variation range of pressure is from -0.027 Pa to -0.014 Pa. When Y = 2, Z = 50.8, the variation range of pressure is from -0.044 Pa to -0.015 Pa. When Y = 2, Z = 51.6, the variation range of pressure is from -0.096 Pa to -0.017 Pa.
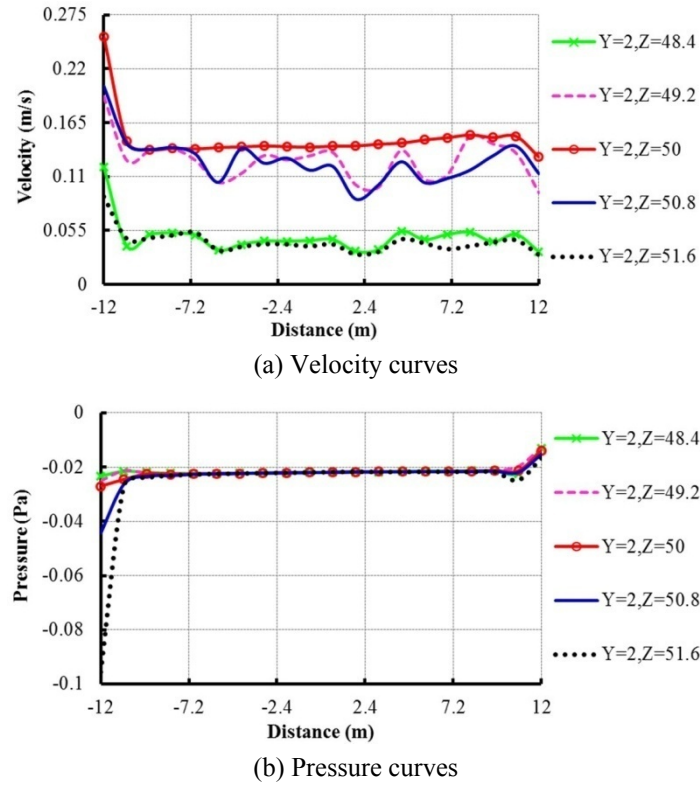
(a) Velocity curves



(b) Pressure curves

Fig. 9 The velocity and pressure curves of the cross passage

(iv) In general, the variation range of pressure in the cross passage is from -0.096 Pa to -0.013 Pa, and the pressure change is little. Moreover, the pressure curves of five probing lines are basically the same, which shows that, in the width direction of the cross passage (Z-direction), the pressure values along the length direction of the cross passage (X-direction) are basically fixed.

(3) As for the five probing lines in the right tunnel (Fig. 7(c)), their velocity curves and pressure curves are shown in Fig. 10.

It can be obtained from Fig. 10:

(i) Fig. 10(a) shows that, when X = 14, Y = 2, the variation range of velocity is from 0 m/s to 0.053 m/s. When X = 16, Y = 2, the variation range of velocity is from 0 m/s to 0.031 m/s. When X = 18, Y = 2, the variation range of velocity is from 0 m/s to 0.023 m/s. When X = 20, Y = 2, the variation range of velocity is from 0 m/s to 0.022 m/s. When X = 22, Y = 2, the variation range of velocity is from 0 m/s to 0.021 m/s.

(ii) In the process of flowing from the cross passage to the right tunnel, the velocity reduces obviously. The variation range of velocity in the right tunnel is from 0 m/s to 0.053 m/s, and the velocity is low speed-based. Overall, the velocity near by the cross passage changes greatly, while it changes gently in other areas. Moreover, the velocity at the working face is 0 m/s. In addition, the velocity is the minimum when X = 22.
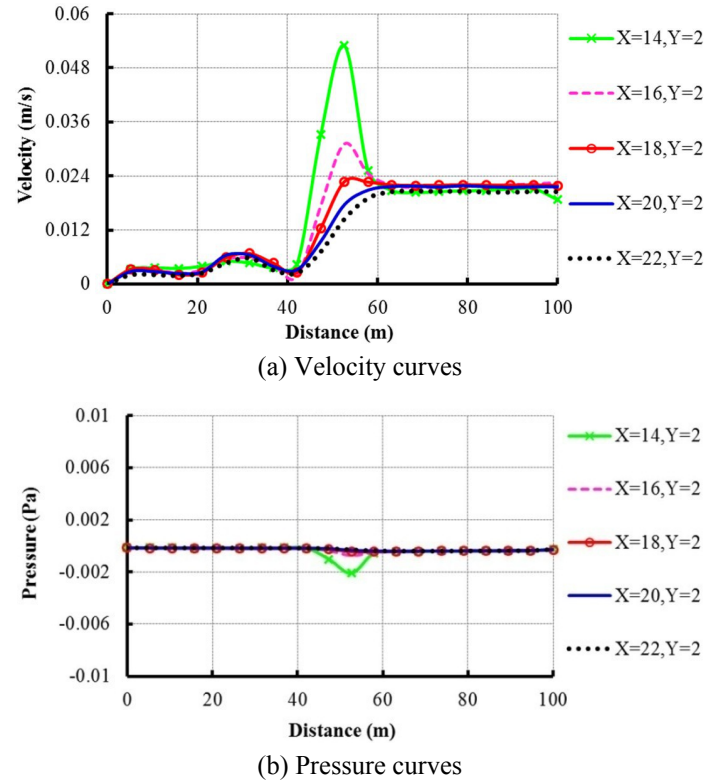
(a) Velocity curves



(b) Pressure curves

Fig. 10 The velocity and pressure curves of the right tunnel

(iii) Fig. 10(b) shows that, when X = 14, Y = 2, the variation range of pressure is from -0.0021 Pa to -0.0002 Pa. When X = 16, Y = 2, the variation range of pressure is from -0.0007 Pa to -0.0002 Pa. When X = 18, Y = 2, the variation range of pressure is from -0.0004 Pa to -0.0002 Pa. When X = 20, Y = 2, the variation range of pressure is from -0.0004 Pa to -0.0002 Pa. When X = 22, Y = 2, the variation range of pressure is from -0.0004 Pa to -0.0001 Pa.

(iv) In the process of flowing from the cross passage to the right tunnel, the pressure reduces obviously. The variation range of pressure in the right tunnel is from -0.0021 Pa to -0.0001 Pa, and the pressure change is little. Moreover, the pressure curves of five probing lines are basically consistent, which shows that, in the width direction of the right tunnel (X-direction), the pressure values along the length direction of the right tunnel (Z-direction) are basically fixed.

(4) As for the five probing broken lines along the height direction (Y-direction) of the tunnel centerline (Fig. 7(d)), their velocity curves and pressure curves are shown in Fig. 11.

It can be obtained from Fig. 11:

(i) Fig. 11(a) shows that, when Y = 0.4, the variation range of velocity is from 0 m/s to 0.234 m/s. When Y = 1.2, the variation range of velocity is from 0 m/s to 0.537 m/s. When Y = 2, the variation range of velocity is from 0 m/s to 0.673 m/s. When Y = 2.8, the

(a) Velocity curves



(b) Pressure curves

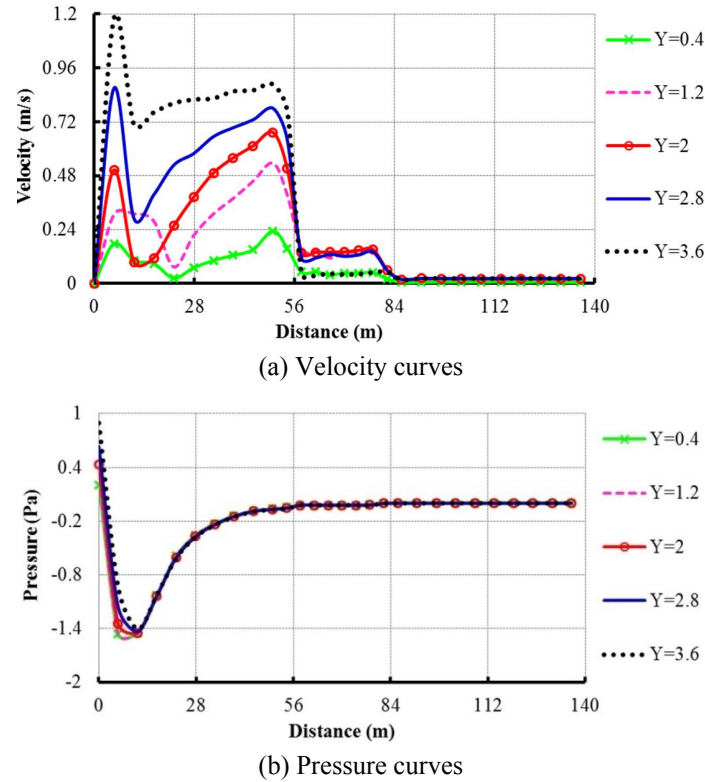Fig. 11 The velocity and pressure curves of Y-direction

variation range of velocity is from 0 m/s to 0.871 m/s. When Y = 3.6, the variation range of velocity is from 0 m/s to 1.18 m/s.

(ii)   In the left tunnel, the velocity increases with the increase of Y, and the velocity is the minimum when Y = 0.4. In the process of flowing from the left tunnel to the cross passage, the velocity reduces obviously, and it is low speed-based. The velocity in the center of the section is the maximum, and then it gradually decreases toward the upper and lower, i.e., the velocity is the maximum when Y = 2, while the velocity is the minimum when Y = 3.6. In the process of flowing from the cross passage to the right tunnel, the velocity decreases obviously, and it is low speed-based. In the right tunnel, the velocity remains unchanged, and the value is close to 0 m/s. Overall, the velocity gets smaller and smaller with the increase of the distance.

(iii)  Fig. 11(b) shows that, when Y = 0.4, the variation range of pressure is from -1.46 Pa to 0.20 Pa. When Y = 1.2, the variation range of pressure is from -1.46 Pa to 0.28 Pa. When Y = 2, the variation range of pressure is from -1.45 Pa to 0.43 Pa. When Y = 2.8, the variation range of pressure is from -1.44 Pa to 0.63 Pa. When Y = 3.6, the variation range of pressure is from -1.41 Pa to 0.90 Pa. The respective maximum positive pressure increases gradually with the increase of Y, and the value is the maximum when Y = 3.6.

(iv)   In general, the pressure changes greatly in the vicinity of the water inrush position, while it changes gently in other areas. The maximum positive pressure appears at the working face of the left tunnel, and the pressure is near 0 Pa at the right tunnel entrance (Outlet 2). In

addition, the pressure curves of five probing broken lines are in good agreement, which shows that, in the height direction of the tunnels (Y-direction), the pressure values along the length direction of the tunnels are basically fixed.

### 4.1.3 The optimized escape routes

(1)  According to the results of velocity curves, the velocity in the center of the section is the maximum, while the velocity at boundaries is the minimum. Therefore, tunnel constructors should first move to the tunnel side wall and then escape quickly when water inrush happens.

(2)  According to the results of pressure curves, the pressure change at the intersection area of the cross passage and the tunnels is large. So, tunnel constructors must not stay here for a short time when escaping.

(3)  Water inrush from floor occurs in the bottom of the left tunnel working face, i.e., Fig. 4(a). During the escaping, if tunnel constructors meet the cross passage, they should pass through it rapidly, turn to the right tunnel without water inrush and run to the entrance.

(4)  Water inrush from floor occurs in the bottom of the left tunnel working face, i.e., Fig. 4(a). The velocity and pressure near by the working face of the right tunnel are small. Thus, if there is not enough time to escape, tunnel constructors can run to the trolley and other equipment in the vicinity of the right tunnel working face.

(5)  Water inrush from floor occurs in the bottom of the left tunnel working face, i.e., Fig. 4(a). The velocity and pressure at the high location of the cross passage are both small, so some rescuing equipment can be set up there.

Combined with this case, the optimized escape routes are shown in Fig. 12.

### 4.2 Case study 2

During the double-line tunnel excavation, water inrush from floor occurs in the middle position of the cross passage because of the impact of mechanical disturbance and other construction factors, i.e., the floor in the middle position of the cross passage is the inlet of water inrush
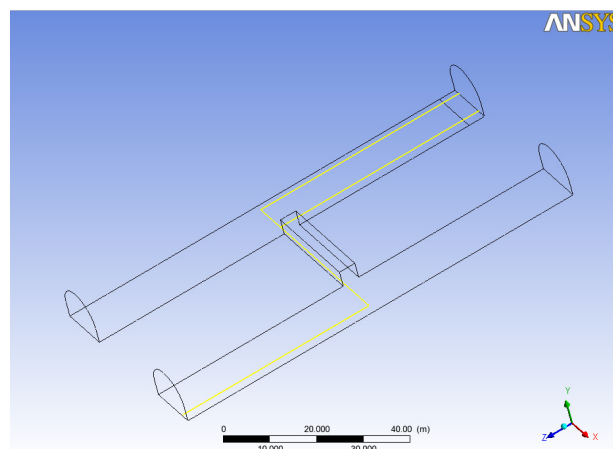


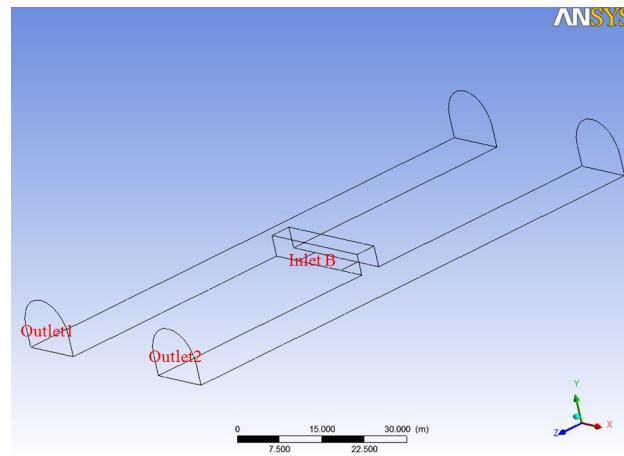Fig. 12 The optimized escape routes (Case 1)

Fig. 13 The water inrush position in the cross passage (Case 2)

(velocity, 2 m/s), and the left and the right tunnel entrances are the outlets of water inrush (pressure, 0 Pa). The scope of water inrush along the length direction of the cross passage (X-direction) is 12 m, and the width direction of the cross passage (Z-direction) is 4 m. The total area of water inrush is 48 $m^2$. As shown in Fig. 13, B is the water inrush position.
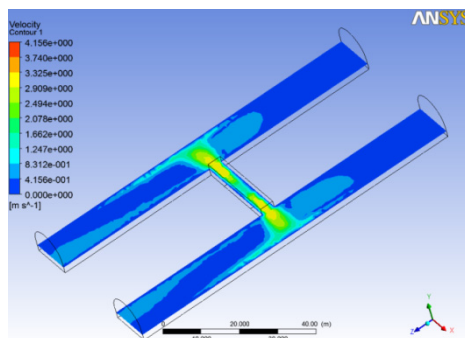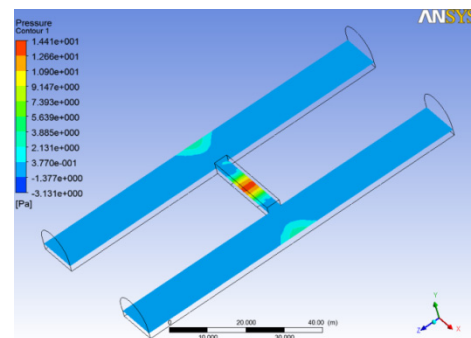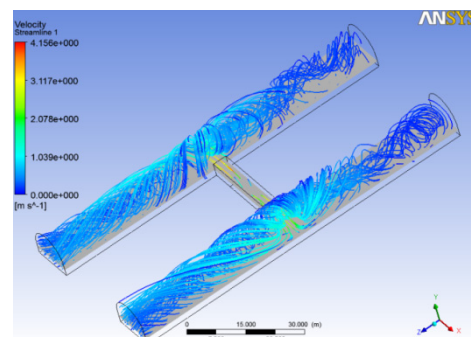


(a) Velocity contour



(b) Pressure contour
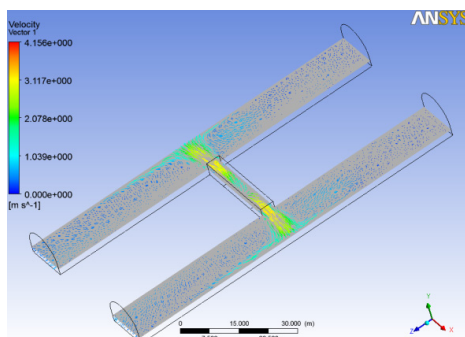


(c) Velocity vector



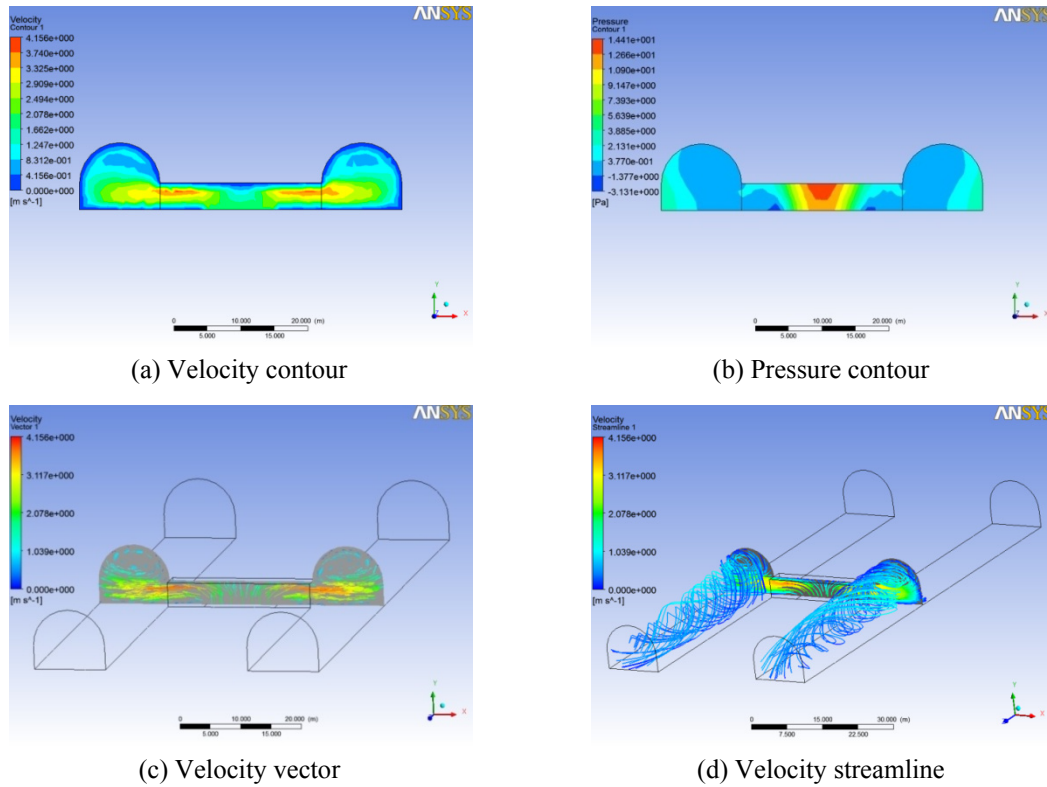(d) Velocity streamline

Fig. 14 Y = 2 section

(a) Velocity contour



(b) Pressure contour



(c) Velocity vector



(d) Velocity streamline

Fig. 15 Z = 50 section

### 4.2.1 Simulated results

Y = 2 section and Z = 50 section are selected as examples. The calculation results are shown in Figs. 14 and 15.

### 4.2.2 Analysis

In order to shows the changes of velocity and pressure in the tunnels more vividly, a series of probing lines are selected. The selection of the probing lines is the same as the case study 1. The details of the probing lines are shown in Table 1, and the corresponding figures are shown in Fig. 7. The probing lines are researched and analyzed.

(1)  As for the five probing lines in the cross passage (Fig. 7(b)), their velocity curves and pressure curves are shown in Fig. 16.

It can be obtained from Fig. 16:

(i)  Fig. 16(a) shows that, when Y = 2, Z = 48.4, the variation range of velocity is from 0.27 m/s to 1.08 m/s. When Y = 2, Z = 49.2, the variation range of velocity is from 1.15 m/s to 3.19 m/s. When Y = 2, Z = 50, the variation range of velocity is from 1.35 m/s to 3.22 m/s. When Y = 2, Z = 50.8, the variation range of velocity is from 1.16 m/s to 3.16 m/s. When Y = 2, Z = 51.6, the variation range of velocity is from 0.39 m/s to 1.25 m/s.

(ii)  The variation range of velocity in the cross passage is from 0.27 m/s to 3.22 m/s. The
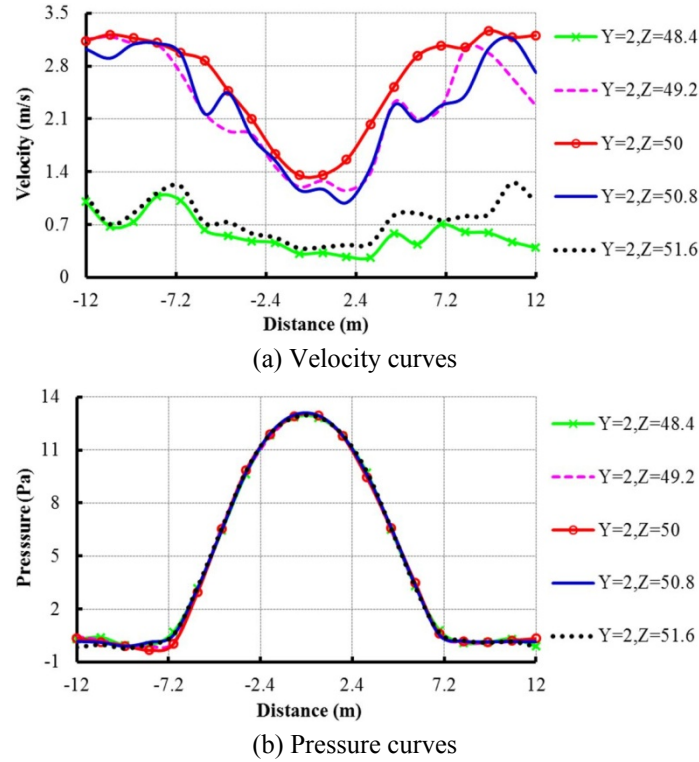
(a) Velocity curves



(b) Pressure curves

Fig. 16 The velocity and pressure curves of the cross passage

velocity is high speed-based, and the changes of velocity are large. Overall, the velocity firstly decreases and then increases with the increase of X. The velocity in the middle position of the cross passage is the minimum, and then it increases gradually toward both ends of the cross passage. It also can be concluded, the velocity in the center of the section is the maximum, and then it decreases gradually toward both sides of the section, i.e., the velocity is the maximum when $Z = 50$, while the velocity is the minimum when $Z = 48.4$.

(iii) Fig. 16(b) shows that, when $Y = 2$, $Z = 48.4$, the variation range of pressure is from -0.06 Pa to 12.9 Pa. When $Y = 2$, $Z = 49.2$, the variation range of pressure is from -0.08 Pa to 12.9 Pa. When $Y = 2$, $Z = 50$, the variation range of pressure is from -0.08 Pa to 12.9 Pa. When $Y = 2$, $Z = 50.8$, the variation range of pressure is from -0.10 Pa to 13.0 Pa. When $Y = 2$, $Z = 51.6$, the variation range of pressure is from -0.02 Pa to 12.9 Pa.

(iv) Overall, the pressure of five probing lines firstly increases and then decreases with the increase of X. The maximum positive pressure appears in the middle position of the cross passage, and then it decreases gradually toward both ends of the cross passage, i.e., the pressure is the maximum when $X = 0$, while the pressure is the minimum when $X = 12$ or -12. In addition, the pressure curves of five probing lines are in good agreement, which shows that, in the width direction of the cross passage (Z-direction), the pressure values along the length direction (X-direction) of the cross passage are fixed.

(2) As for the five probing lines in the left tunnel (Fig. 7(a)), their velocity curves and pressure curves are shown in Fig. 17.
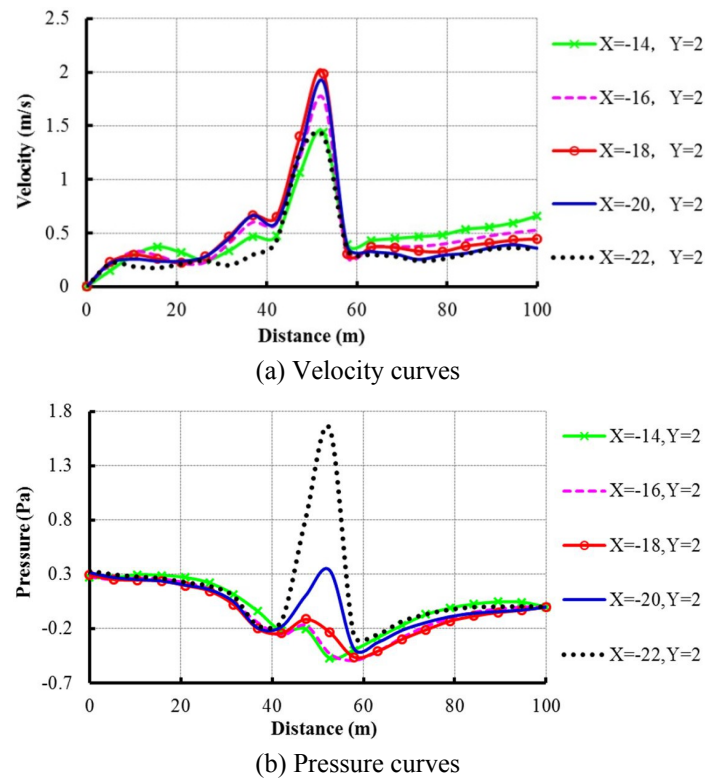
(a) Velocity curves



(b) Pressure curves

Fig. 17 The velocity and pressure curves of the left tunnel

It can be obtained from Fig. 17:

(i)  Fig. 17(a) shows that, when X = -14, Y = 2, the variation range of velocity is from 0 m/s to 1.44 m/s. When X = -16, Y = 2, the variation range of velocity is from 0 m/s to 1.75 m/s. When X = -18, Y = 2, the variation range of velocity is from 0 m/s to 1.99 m/s. When X = -20, Y = 2, the variation range of velocity is from 0 m/s to 1.91 m/s. When X = -22, Y = 2, the variation range of velocity is from 0 m/s to 1.4 m/s.

(ii)  In the process of flowing from the cross passage to the left tunnel, the velocity reduces obviously. The variation range of velocity in the left tunnel is from 0 m/s to 1.99 m/s, and the velocity is low speed-based. Overall, the velocity firstly increases and then decreases with the increase of the distance. The velocity at the working face is 0 m/s, and it is larger in the vicinity of the cross passage, i.e., the velocity is the minimum when Z = 0, while the velocity is the maximum when Z = 50. It also can be concluded, among the five selected probing lines, the velocity is the minimum when X = -22.

(iii)  Fig. 17(b) shows that, when X = -14, Y = 2, the variation range of pressure is from -0.47 Pa to 0.30 Pa. When X = -16, Y = 2, the variation range of pressure is from -0.49 Pa to 0.28 Pa. When X = -18, Y = 2, the variation range of pressure is from -0.46 Pa to 0.30 Pa. When X = -20, Y = 2, the variation range of pressure is from -0.38 Pa to 0.34 Pa. When X = -22, Y = 2, the variation range of pressure is from -0.26 Pa to 1.64 Pa.

(iv)  When the variation range of Z is from 0 to 40, the pressure decreases gradually. The pressure in the center of the section is the minimum, and then it increases gradually toward

both sides of the section. When the variation range of Z is from 40 to 60, the pressure first increases and then decreases. The pressure is the maximum when X = -22, while it is the minimum when X = -14. When the variation range of Z is from 60 to 100, the pressure increases gradually, and it becomes 0 Pa at the left tunnel entrance (Outlet 1). The pressure in the center of the section is the minimum, and then it increases gradually toward both sides of the section. In general, the pressure changes greatly in the vicinity of the cross passage, while it changes gently in other areas.

(3)   As for the five probing lines in the right tunnel (Fig. 7(c)), their velocity curves and pressure curves are shown in Fig. 18.

It can be obtained from Fig. 18:
(i)   Fig. 18(a) shows that, when X = 14, Y = 2, the variation range of velocity is from 0 m/s to 1.42 m/s. When X = 16, Y = 2, the variation range of velocity is from 0 m/s to 1.82 m/s. When X = 18, Y = 2, the variation range of velocity is from 0 m/s to 1.90 m/s. When X = 20, Y = 2, the variation range of velocity is from 0 m/s to 1.92 m/s. When X = 22, Y = 2, the variation range of velocity is from 0 m/s to 1.39 m/s.
(ii)   In the process of flowing from the cross passage to the right tunnel, the velocity reduces obviously. The variation range of velocity in the right tunnel is from 0 m/s to 1.92 m/s, and the velocity is low speed-based. Overall, the velocity firstly increases and then decreases
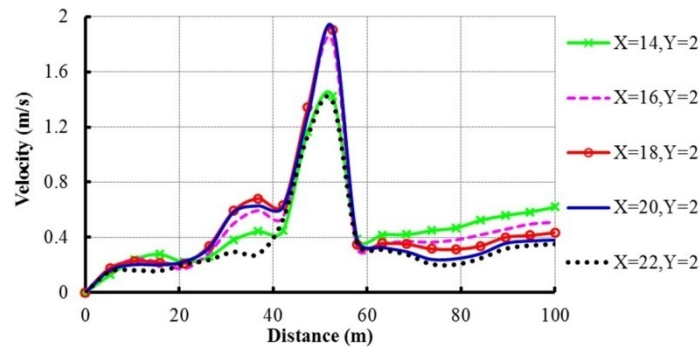


(a) Velocity curves
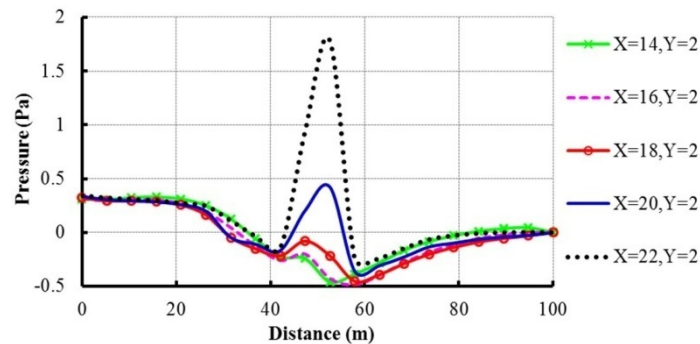


(b) Pressure curves

Fig. 18 The velocity and pressure curves of the right tunnel

with the increase of the distance. The velocity at the working face is 0 m/s, and it is larger in the vicinity of the cross passage, i.e., the velocity is the minimum when $Z = 0$, while the velocity is the maximum when $Z = 50$. In addition, it also can be concluded, among the five selected probing lines, the velocity is the minimum when $X = 22$.

(iii) Fig. 18(b) shows that, when $X = 14$, $Y = 2$, the variation range of pressure is from -0.46 Pa to 0.33 Pa. When $X = 16$, $Y = 2$, the variation range of pressure is from -0.49 Pa to 0.31 Pa. When $X = 18$, $Y = 2$, the variation range of pressure is from -0.45 Pa to 0.32 Pa. When $X = 20$, $Y = 2$, the variation range of pressure is from -0.36 Pa to 0.42 Pa. When $X = 22$, $Y = 2$, the variation range of pressure is from -0.25 Pa to 1.78 Pa.

(iv) When the variation range of $Z$ is from 0 to 40, the pressure decreases gradually. The pressure in the center of the section is the minimum, and then it increases gradually toward both sides of the section. When the variation range of $Z$ is from 40 to 60, the pressure first increases and then decreases. The pressure is the maximum when $X = 22$, and it is the minimum when $X = 14$. When the variation range of $Z$ is from 60 to 100, the pressure increases gradually, and it becomes 0 Pa at the right tunnel entrance (Outlet 2). The pressure in the center of the section is the minimum, and then it increases gradually toward both sides of the section. In general, the pressure changes greatly in the vicinity of the cross passage, while it changes gently in other areas.

(4)   As for the five probing broken lines along the height direction (Y-direction) of the tunnel centerline (Fig. 7(d)), their velocity curves and pressure curves are shown in Fig. 19.

The following conclusions can be obtained from Fig. 19:

(i)   Fig. 19(a) shows that, when $Y = 0.4$, the variation range of velocity is from 0 m/s to 1.15 m/s. When $Y = 1.2$, the variation range of velocity is from 0 m/s to 2.56 m/s. When $Y = 2$, the variation range of velocity is from 0 m/s to 3.26 m/s. When $Y = 2.8$, the variation range of velocity is from 0 m/s to 3.71 m/s. When $Y = 3.6$, the variation range of velocity is from 0 m/s to 3.02 m/s.

(ii)   In the cross passage, the velocity changes greatly, and it varies in a wave shape. The velocity is larger on both ends of the cross passage. Moreover, among the five selected probing lines, the velocity is the minimum when $Y = 0.4$. In the process of flowing from the cross passage to the left tunnel, the velocity reduces quickly, and then it reduces slowly in the left tunnel. The velocity becomes 0 m/s at the working face. Among the five selected probing lines, the velocity is the minimum when $Y = 0.4$. In the process of flowing from the cross passage to the right tunnel, the velocity reduces quickly, and then it changes gently in the right tunnel. Moreover, the velocity is low speed-based. Among the five selected probing lines, the velocity is the minimum when $Y = 0.4$ or 3.6.

(iii) Fig. 19(b) shows that, when $Y = 0.4$, the variation range of pressure is from -0.45 Pa to 11.0 Pa. When $Y = 1.2$, the variation range of pressure is from -0.42 Pa to 11.2 Pa. When $Y = 2$, the variation range of pressure is from -0.45 Pa to 11.8 Pa. When $Y = 2.8$, the variation range of pressure is from -0.49 Pa to 12.3 Pa. When $Y = 3.6$, the variation range of pressure is from -0.52 Pa to 12.8 Pa.

(iv) In general, with the increase of the distance to the left tunnel working face, the pressure first increases and then decreases. The pressure changes greatly in the cross passage, and it reaches its maximum positive pressure in the middle position of the cross passage. More-
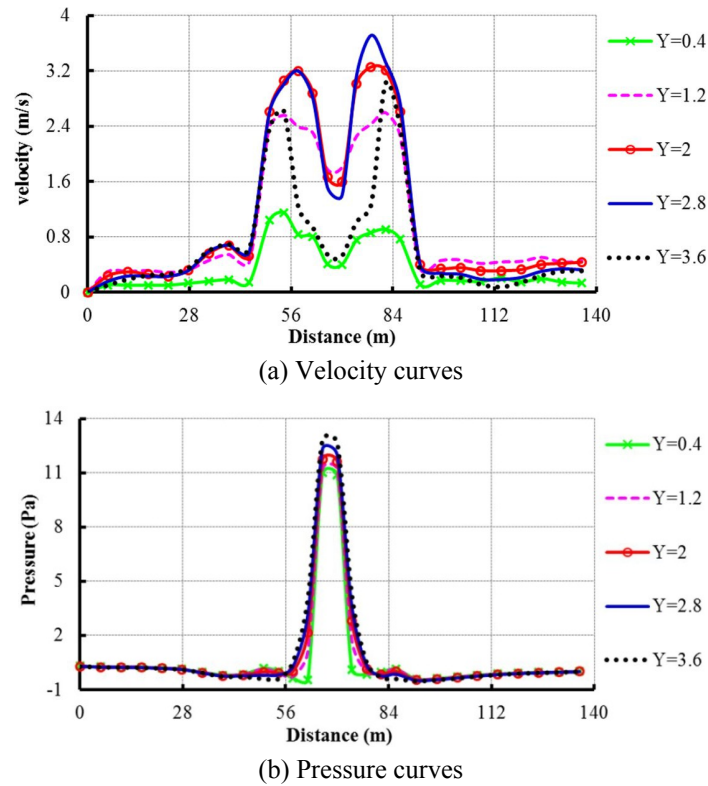
(a) Velocity curves



(b) Pressure curves

Fig. 19 The velocity and pressure curves of Y-direction

over, the maximum positive pressure increases with the increase of Y, i.e., the value is the maximum when Y = 3.6. The pressure changes gently in the left and the right tunnels, and the pressure at the left and right tunnel entrances is close to 0 Pa. In addition, the pressure curves of five probing broken lines are basically the same, which shows that, in the height direction of the tunnels (Y-direction), the pressure values along the length direction of the tunnels are basically fixed.

### 4.2.3 The optimized escape routes

(1) According to the results of velocity curves, the velocity in the center of the section is the maximum, while it at boundaries is the minimum. Therefore, tunnel constructors should first move to the tunnel side wall and then escape quickly when water inrush happens.

(2) According to the results of pressure curves, the pressure change at the intersection area of the cross passage and the tunnels is large. So, tunnel constructors must not stay here for a short time when escaping.

(3) Water inrush from floor occurs in the middle position of the cross passage, i.e., Fig. 13(b). During the escaping, tunnel constructors in the cross passage should pass through it rapidly, turn to the left tunnel (or the right tunnel) and run to the entrance.

(4) Water inrush from floor occurs in the middle position of the cross passage, i.e., Fig. 13(b). During the escaping, tunnel constructors in the left tunnel (or the right tunnel) should first move to the tunnel side wall and then run to the entrance.

(5)  Water inrush from floor occurs in the middle position of the cross passage, i.e., Fig. 13(b). The velocity and pressure near by the working faces (the left tunnel and the right tunnel) are both small. Thus, if there is not enough time to escape, tunnel constructors can run to the trolley and other equipment in the vicinity of the working faces (the left tunnel and the right tunnel).

Combined with this case, the optimized escape routes are shown in Fig. 20.

### 4.3 Case study 3

The following case may be encountered during the double-line tunnel excavation. In the process of the left tunnel excavation, the tunneling cannot be carried out due to the effects of geological conditions and other factors. At this time, the right tunnel should first be excavated, and then both ends of the left tunnel are further excavated after passing through the cross passage.
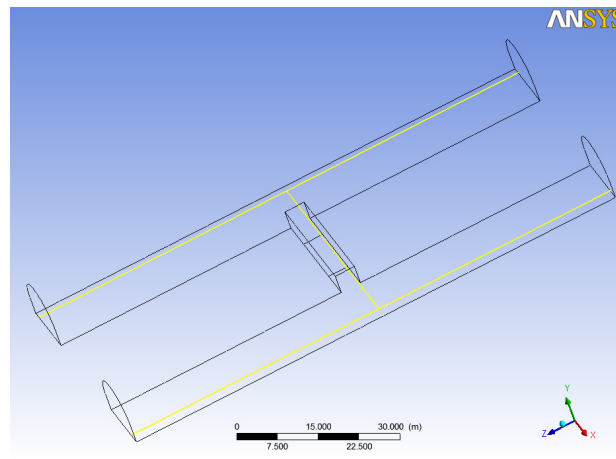


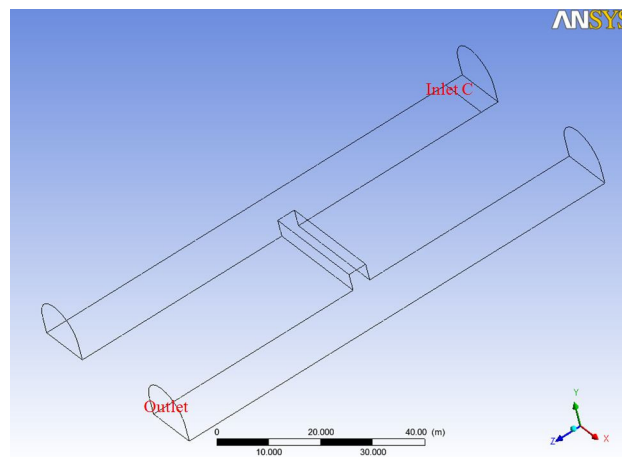Fig. 20 The optimized escape routes (Case 2)



Fig. 21 The water inrush position in the left tunnel (Case 3)

During the left tunnel excavation, water inrush from floor occurs in the bottom of the working face (away from the left tunnel entrance), i.e., the floor below the left tunnel working face is the inlet of water inrush (velocity, 2 m/s), and the right tunnel entrance is the outlet of water inrush (pressure, 0 Pa). The scope of water inrush along the length direction of the left tunnel (Z-direction) is 4 m, and the width direction of the left tunnel (X-direction) is 12 m. The total area of water inrush is 48 m². As shown in Fig. 21, C is the water inrush position.
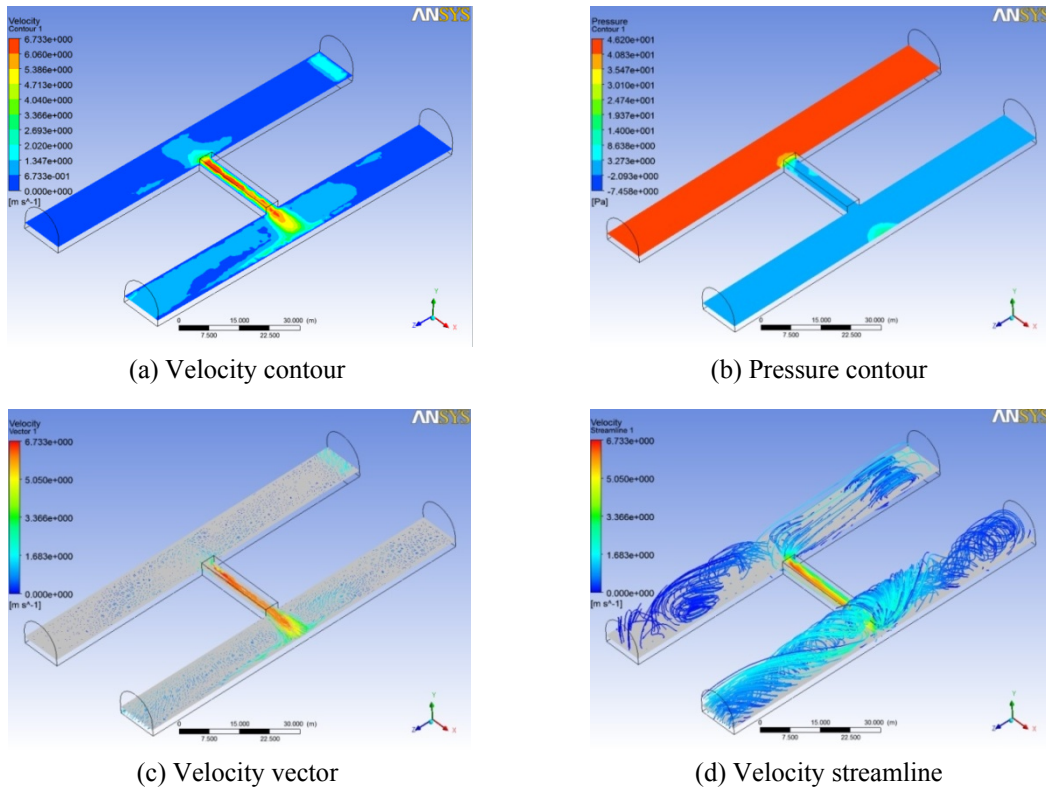


(a) Velocity contour



(b) Pressure contour



(c) Velocity vector



(d) Velocity streamline

Fig. 22 Y = 2 section
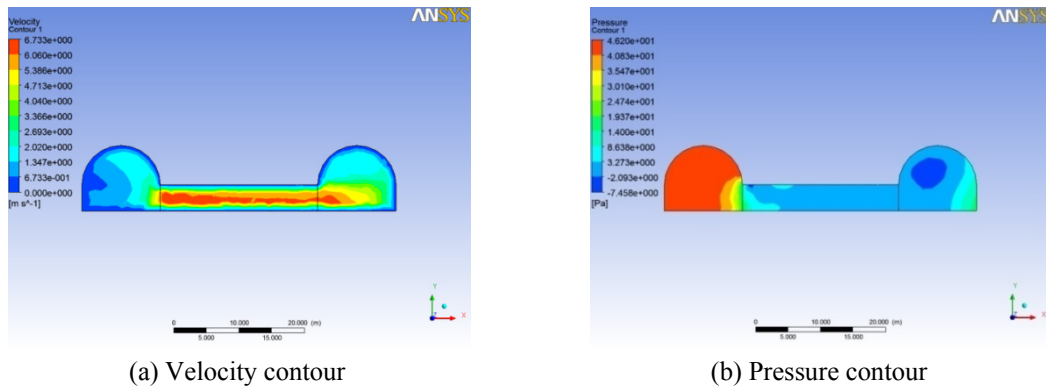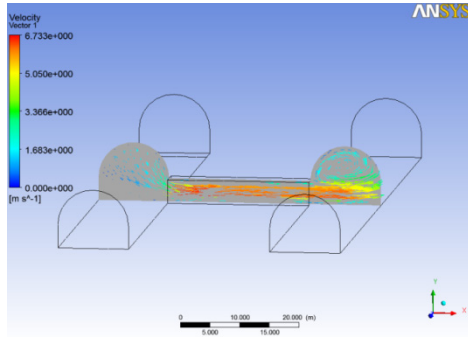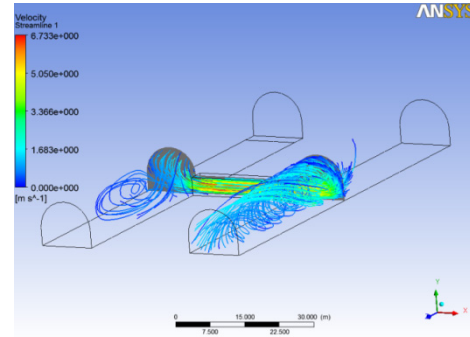


(a) Velocity contour



(b) Pressure contour

Fig. 23 Z = 50 section

(c) Velocity vector



(d) Velocity streamline

Fig. 23 Continued

### 4.3.1 Simulated results

Y = 2 section and Z = 50 section are selected as examples. The calculation results are shown in Figs. 22 and 23.

### 4.3.2 Analysis

In order to shows the changes of velocity and pressure in the tunnels more vividly, a series of probing lines are selected. The selection of the probing lines is identical with the case study 1. The details of the probing lines are shown in Table 1, and the corresponding figures are shown in Fig. 7. The probing lines are researched and analyzed.

(1)   As for the five probing lines in the left tunnel (Fig. 7(a)), their velocity curves and pressure curves are shown in Fig. 24.

It can be obtained from Fig. 24:

(i)   Fig. 24(a) shows that, when X = -14, Y = 2, the variation range of velocity is from 0 m/s to 2.08 m/s. When X = -16, Y = 2, the variation range of velocity is from 0 m/s to 1.25 m/s. When X = -18, Y = 2, the variation range of velocity is from 0 m/s to 0.99 m/s. When X = -20, Y = 2, the variation range of velocity is from 0 m/s to 0.89 m/s. When X = -22, Y = 2, the variation range of velocity is from 0 m/s to 0.80 m/s.

(ii)   Overall, the variation range of velocity in the left tunnel is from 0 m/s to 2.08 m/s, and the velocity is high speed-based. The velocity changes greatly, and it varies in a wave shape. The velocity near by the cross passage is larger, and then it decreases gradually toward both ends of the left tunnel, and the velocity is 0 m/s at the two working faces. It also can be concluded, the velocity close to one side of the cross passage is the maximum, and then it decreases gradually toward the other side, i.e., the velocity is the maximum when X = -14, while the velocity is the minimum when X = -22.

(iii)   Fig. 24(b) shows that, when X = -14, Y = 2, the variation range of pressure is from 39.2 Pa to 44.6 Pa. When X = -16, Y = 2, the variation range of pressure is from 42.1 Pa to 44.6 Pa. When X = -18, Y = 2, the variation range of pressure is from 42.6 Pa to 44.6 Pa. When X = -20, Y = 2, the variation range of pressure is from 42.3 Pa to 44.6 Pa. When X = -22, Y = 2, the variation range of pressure is from 42.2 Pa to 44.6 Pa.

(iv)   In general, the variation range of pressure in the left tunnel is from 39.2 Pa to 44.6 Pa, and
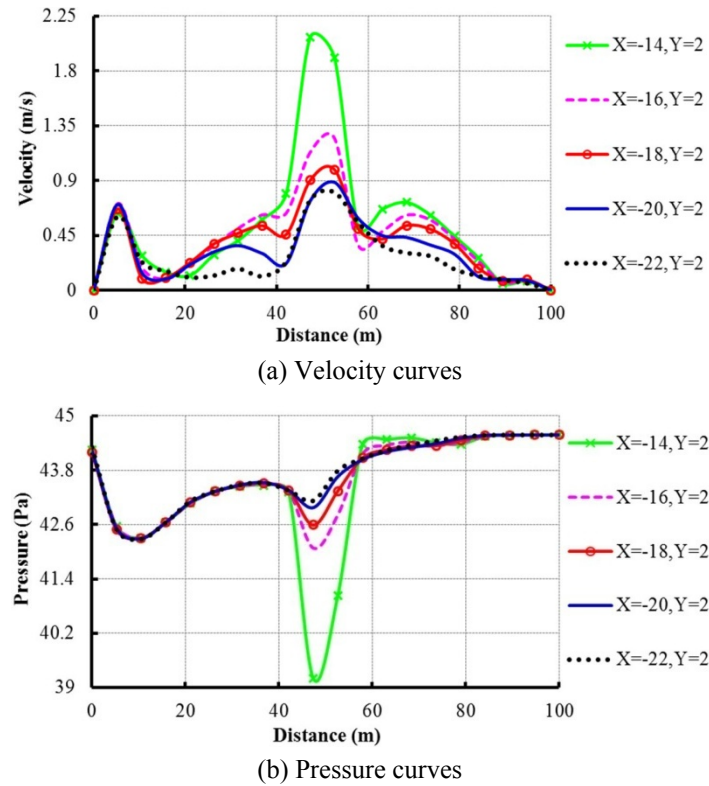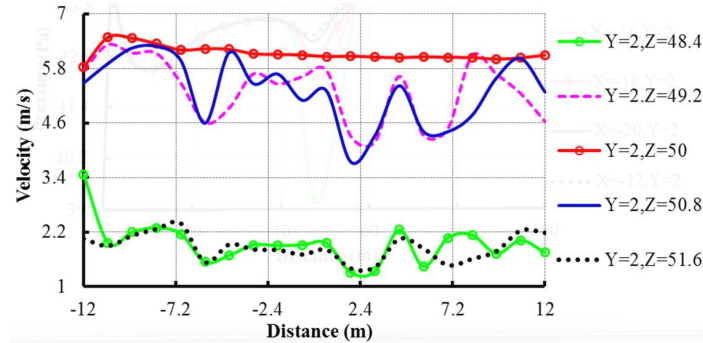
(a) Velocity curves



(b) Pressure curves

Fig. 24 The velocity and pressure curves of the left tunnel

the pressure is high-pressure based. The pressure changes greatly, and it varies in a wave shape. When the variation range of Z is from 0 to 40, the pressure first decreases and then increases gradually. The pressure curves of five probing lines are in good agreement. When the variation range of Z is from 40 to 60, the pressure first decreases and then increases rapidly. The pressure close to one side of the cross passage is the minimum, and then it increases gradually toward the other side, i.e., the pressure is the minimum when X = -14, while the pressure is the maximum when X = -22. When the variation range of Z is from 60 to 100, the pressure continues to increase slowly, and it reaches its maximum value (44.6 Pa) when Z = 100. Moreover, the pressure curves of five probing lines are basically consistent.

(2)  As for the five probing lines in the cross passage (Fig. 7(b)), their velocity curves and pressure curves are shown in Fig. 25.

It can be obtained from Fig. 25:

(i)   Fig. 25(a) shows that, when Y = 2, Z = 48.4, the variation range of velocity is from 1.30 m/s to 3.47 m/s. When Y = 2, Z = 49.2, the variation range of velocity is from 4.19 m/s to 6.32 m/s. When Y = 2, Z = 50, the variation range of velocity is from 5.83 m/s to 6.49 m/s. When Y = 2, Z = 50.8, the variation range of velocity is from 4.33 m/s to 6.29 m/s. When Y = 2, Z = 51.6, the variation range of velocity is from 1.40 m/s to 2.39 m/s.

(a) Velocity curves
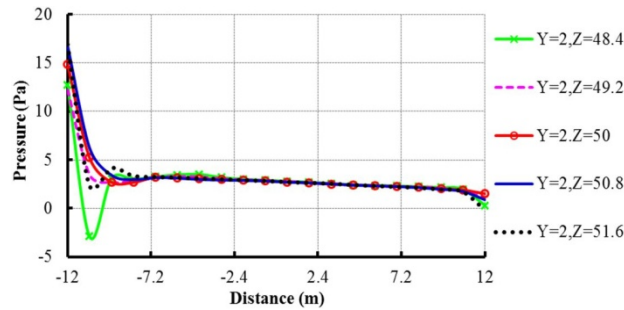


(b) Pressure curves

Fig. 25 The velocity and pressure curves of the cross passage

(ii) In the process of flowing from the left tunnel to the cross passage, the velocity increases rapidly. The variation range of velocity in the cross passage is from 1.30 m/s to 6.49 m/s, and the velocity is high speed-based. It also can be concluded, the velocity in the center of the section is the maximum, and then it decreases gradually toward both sides of the section, i.e., the velocity is the maximum when Z = 50, while the velocity is the minimum when Z = 51.6.

(iii) Fig. 25(b) shows that, when Y = 2, Z = 48.4, the variation range of pressure is from -2.90 Pa to 12.7 Pa. When Y = 2, Z = 49.2, the variation range of pressure is from 1.13 Pa to 12.3 Pa. When Y = 2, Z = 50, the variation range of pressure is from 1.50 Pa to 14.9 Pa. When Y = 2, Z = 50.8, the variation range of pressure is from 0.88 Pa to 16.8 Pa. When Y = 2, Z = 51.6, the variation range of pressure is from -1.76 Pa to 16.9 Pa.

(iv) In the process of flowing from the left tunnel to the cross passage, the pressure decreases rapidly. The variation range of pressure in the cross passage is from -2.90 Pa to 16.9 Pa. Overall, the pressure is the maximum at the starting point of the cross passage, and then it decreases gradually with the increase of X. When the variation range of X is from -12 to -9, the pressure sharply decreases. The pressure close to one side of the water inrush is the minimum, and then it increases gradually towards the other side, i.e., the pressure is the minimum when Z = 48.4, while the pressure is the maximum when Z = 50.8. When the variation range of X is from -9 to 12, the pressure continues to decrease slowly, and the pressure curves of five probing lines are in good agreement.
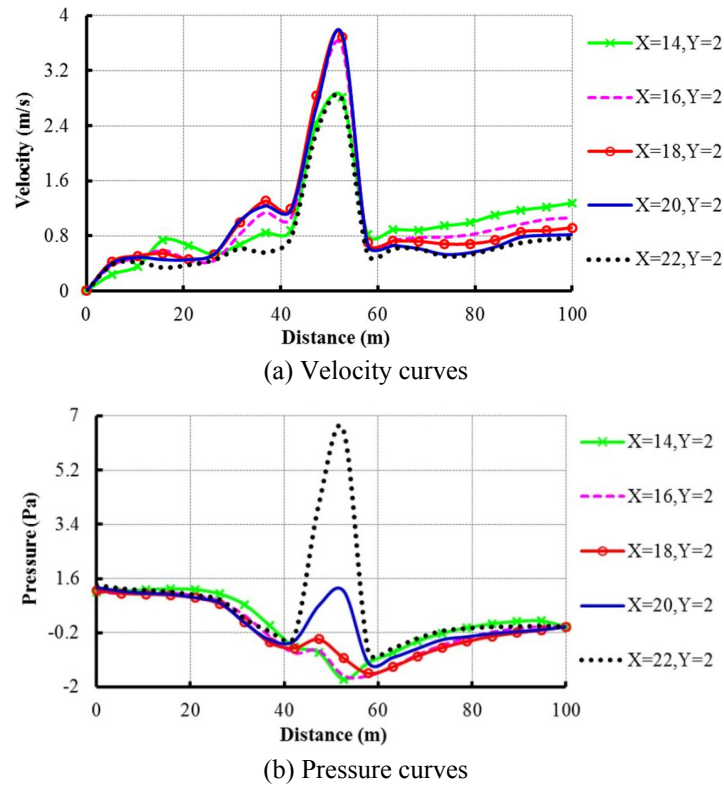
(a) Velocity curves



(b) Pressure curves

Fig. 26 The velocity and pressure curves of the right tunnel

(3) As for the five probing lines in the right tunnel (Fig. 7(c)), their velocity curves and pressure curves are shown in Fig. 26.

It can be obtained from Fig. 26:

(i) Fig. 26(a) shows that, when X = 14, Y = 2, the variation range of velocity is from 0 m/s to 2.81 m/s. When X = 16, Y = 2, the variation range of velocity is from 0 m/s to 3.55 m/s. When X = 18, Y = 2, the variation range of velocity is from 0 m/s to 3.69 m/s. When X = 20, Y = 2, the variation range of velocity is from 0 m/s to 3.73 m/s. When X = 22, Y = 2, the variation range of velocity is from 0 m/s to 2.79 m/s.

(ii) In the process of flowing from the cross passage to the right tunnel, the velocity reduces obviously. The variation range of velocity in the right tunnel is from 0 m/s to 3.73 m/s, and the velocity is high speed-based. Overall, the velocity firstly increases and then decreases with the increase of the distance. The velocity at the working face is 0 m/s, and the velocity near by the cross passage is relatively high, i.e., the velocity is the minimum when Z = 0, while the velocity is the maximum when Z = 50. It also can be concluded, among the five selected probing lines, the velocity is the minimum when X = 22.

(iii) Fig. 26(b) shows that, when X = 14, Y = 2, the variation range of pressure is from -1.74 Pa to 1.26 Pa. When X = 16, Y = 2, the variation range of pressure is from -1.63 Pa to 1.16 Pa. When X = 18, Y = 2, the variation range of pressure is from -1.55 Pa to 1.21 Pa. When X = 20, Y = 2, the variation range of pressure is from -1.20 Pa to 1.30 Pa. When X = 22, Y = 2,
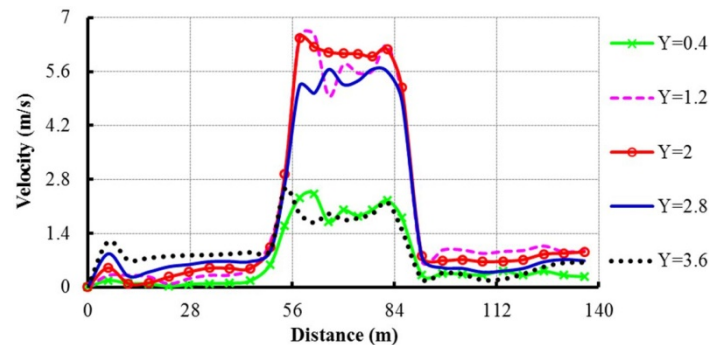
the variation range of pressure is from -0.85 Pa to 6.50 Pa.

(iv) In the process of flowing from the cross passage to the right tunnel, the pressure reduces obviously. The variation range of pressure in the right tunnel is from -1.74 Pa to 6.50 Pa, and the pressure is low pressure-based. When the variation range of Z is from 0 to 40, the pressure gradually decreases. The pressure in the center of the section is the minimum, and then it increases gradually toward both sides of the section. When the variation range of Z is from 40 to 60, the pressure first increases and then decreases. The pressure is the maximum when X = 22, while the pressure is the minimum when X = 14. When the variation range of Z is from 60 to 100, the pressure increases gradually and it becomes 0 Pa at the right tunnel entrance (Outlet). Moreover, the pressure in the center of the section is the minimum, and then it gradually toward both sides of the section. In general, the pressure changes greatly in the vicinity of the cross passage, while it changes gently in other areas.

(4) As for the five probing broken lines along the height direction (Y-direction) of the tunnel centerline (Fig. 7(d)), their velocity curves and pressure curves are shown in Fig. 27.

It can be obtained from Fig. 27:

(i) Fig. 27(a) shows that, when Y = 0.4, the variation range of velocity is from 0 m/s to 2.43 m/s. When Y = 1.2, the variation range of velocity is from 0 m/s to 6.58 m/s. When Y = 2,



(a) Velocity curves
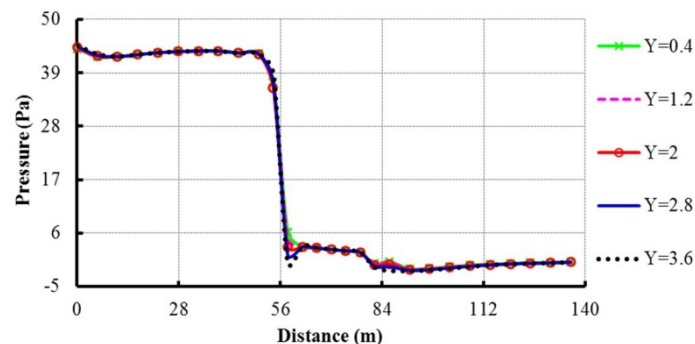


(b) Pressure curves

Fig. 27 The velocity and pressure curves of Y-direction

the variation range of velocity is from 0 m/s to 6.47 m/s. When $Y = 2.8$, the variation range of velocity is from 0 m/s to 5.66 m/s. When $Y = 3.6$, the variation range of velocity is from 0 m/s to 2.56 m/s.

(i)　The velocity changes more gently in the left tunnel, and the velocity is the minimum when $Y = 0.4$. In the process of flowing from the left tunnel to the cross passage, the velocity increases obviously. In the cross passage, the velocity in the center of the section is the maximum, and then it decreases gradually toward the upper and lower, i.e., the velocity is the maximum when $Y = 2$, while the velocity is the minimum when $Y = 3.6$. In the process of flowing from the cross passage to the right tunnel, the velocity decreases rapidly. The velocity changes gently in the right tunnel, and the velocity is lower when $Y = 0.4$ or 3.6.

(ii)　Fig. 27(b) shows that, when $Y = 0.4$, the variation range of pressure is from -0.95 Pa to 44 Pa. When $Y = 1.2$, the variation range of pressure is from -0.99 Pa to 44.1 Pa. When $Y = 2$, the variation range of pressure is from -0.77 Pa to 44.2 Pa. When $Y = 2.8$, the variation range of pressure is from -0.90 Pa to 44.4 Pa. When $Y = 3.6$, the variation range of pressure is from -0.90 Pa to 44.7 Pa.

(iii)　The pressure keeps unchanged in the left tunnel. In the process of flowing from the left tunnel to the cross passage, the pressure reduces obviously. Then, in the process of flowing from the cross passage to the right tunnel, the pressure continues to reduce. In general, the pressure at the left tunnel working face is the maximum, and then it decreases gradually along the direction of water inrush. In addition, the pressure curves of five probing lines are in good agreement, which shows that, in the height direction of the tunnels (Y-direction), the pressure values along the length direction of the tunnel are fixed.

### 4.3.3 The optimized escape routes

(1)　According to the results of velocity curves, the velocity in the center of the section is the maximum, while the velocity at boundaries is the minimum. Therefore, tunnel constructors should first move to the tunnel side wall and then escape quickly when water inrush happens.

(2)　According to the results of pressure curves, the pressure change at the intersection area of the cross passage and the tunnels is large. So, tunnel constructors must not stay here for a short time when escaping.

(3)　Water inrush from floor occurs in the bottom of the left tunnel working face, i.e., Fig. 21(c). During the escaping, if tunnel constructors meet the cross passage, then they should pass through it rapidly, turn to the right tunnel without water inrush and run to the entrance.

(4)　Water inrush from floor occurs in the bottom of the left tunnel working face, i.e., Fig. 21(c). The velocity near by the left tunnel working face (close to the left tunnel entrance) is small. Thus, if there is not enough time to escape, tunnel constructors can run to the trolley and other equipment in the vicinity of the left tunnel working face (close to the left tunnel entrance).

(5)　Water inrush from floor occurs in the bottom of the left tunnel working face, i.e., Fig. 21(c). The velocity nearby the right tunnel working face is 0 m/s. Thus, if there is not enough time to escape, tunnel constructors can run to the trolley and other equipment in the vicinity of the right tunnel working face.

(6)　Water inrush from floor occurs in the bottom of the left tunnel working face, i.e., Fig. 21(c). The velocity and pressure on the high location of the cross passage are both small, so some rescuing equipment can be set up there.
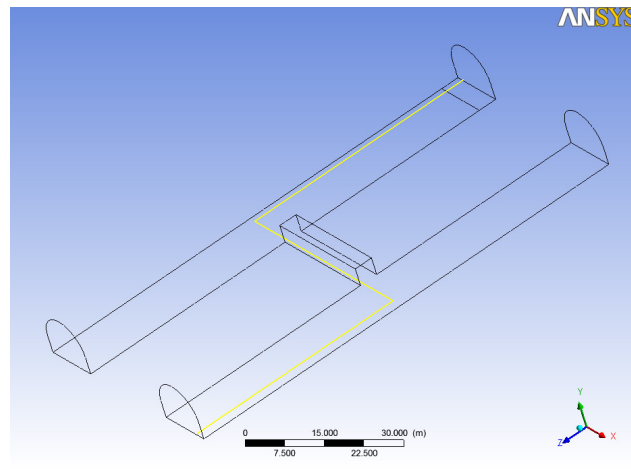
Fig. 28 The optimized escape routes (Case 3)

Combined with this case, the optimized escape routes are shown in Fig. 28.

### 4.4 Case study 4

The excavation situation of this case is identical with the case 3. During the double-line tunnel excavation, water inrush from floor occurs in the middle position of the cross passage because of the impact of mechanical disturbance and other construction factors, i.e., the floor in the middle position of the cross passage is the inlet of water inrush (velocity, 2 m/s), and the right tunnel entrance is the outlet of water inrush (pressure, 0 Pa). The scope of water inrush along the length direction of the cross passage (X-direction) is 12 m, and the width direction of the cross passage (Z-direction) is 4 m. The total area of water inrush is 48 m$^2$. As shown in Fig. 29, D is the water inrush position.
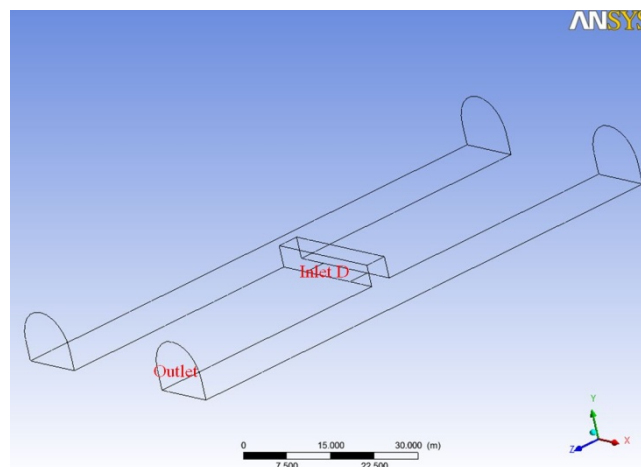


Fig. 29 The optimized escape routes (Case 4)
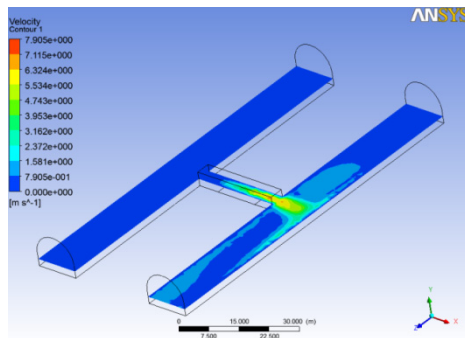
(a) Velocity contour
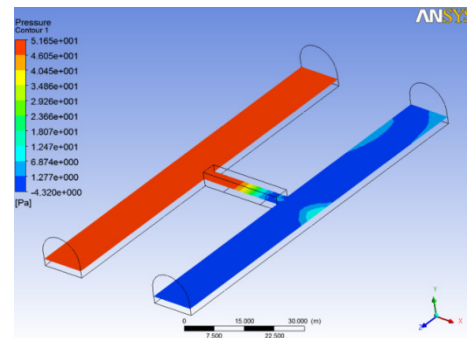


(b) Pressure contour
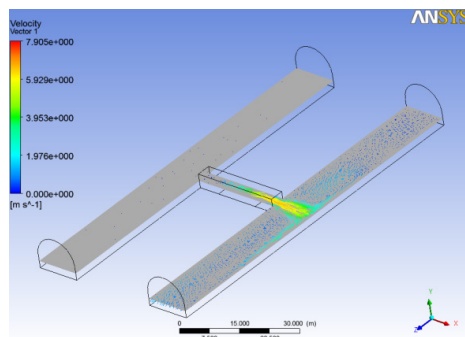


(c) Velocity vector
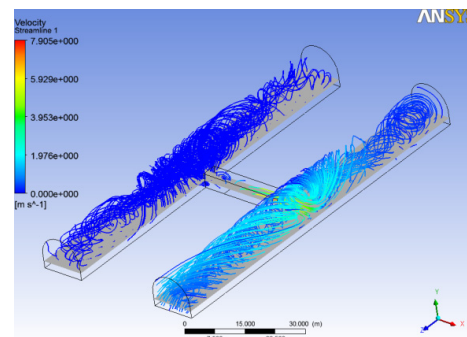


(d) Velocity streamline

Fig. 30 Y = 2 section

### 4.4.1 Simulated results

Y = 2 section and Z = 50 section are selected as examples. The calculation results are shown in Figs. 30 and 31.

### 4.4.2 Analysis

In order to shows the changes of velocity and pressure in the tunnels more vividly, a series of
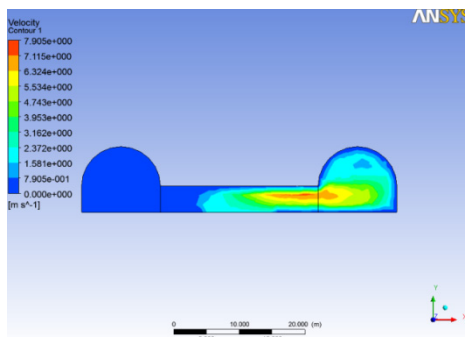


(a) Velocity contour
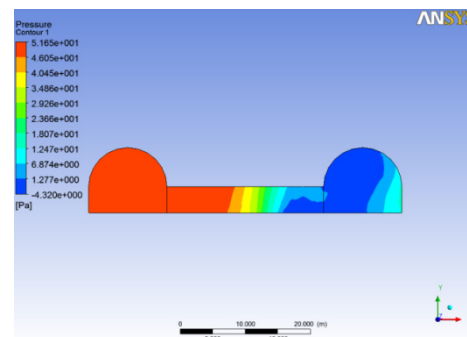


(b) Pressure contour

Fig. 31 Z = 50 section
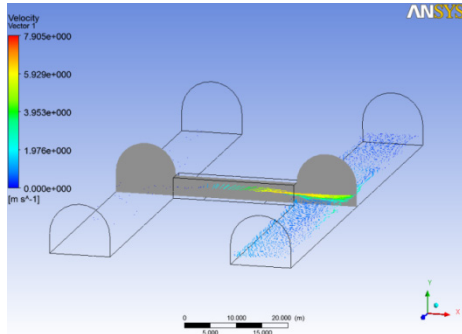
(c) Velocity vector
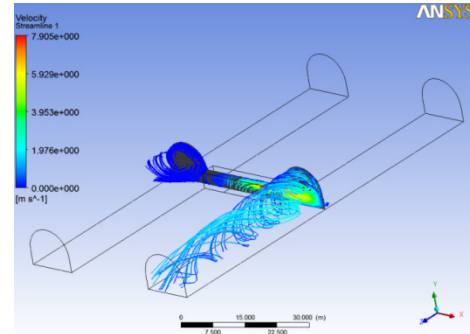


(d) Velocity streamline

Fig. 31 Continued

probing lines are selected. The selection of the probing lines is the same as the case study 1. The details of the probing lines are shown in Table 1, and the corresponding figures are shown in Fig. 7. The probing lines are researched and analyzed.

(1) As for the five probing lines in the cross passage (Fig. 7(b)), their velocity curves and pressure curves are shown in Fig. 32.
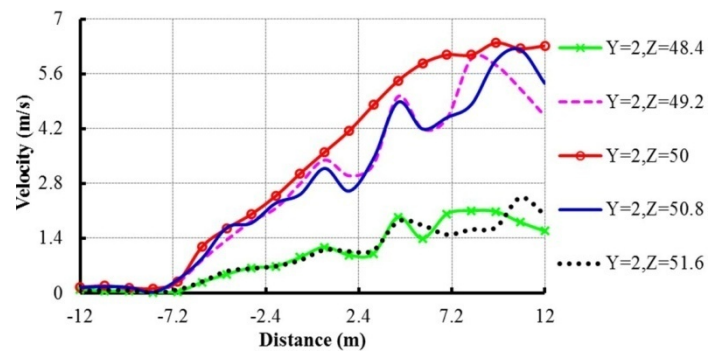


(a) Velocity curves
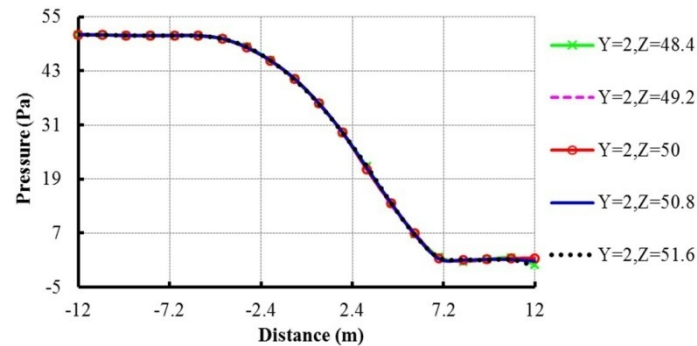


(b) Pressure curves

Fig. 32 The velocity and pressure curves of the cross passage

It can be obtained from Fig. 32:

(i)   Fig. 32(a) shows that, when Y = 2, Z = 48.4, the variation range of velocity is from 0.02 m/s to 2.11 m/s. When Y = 2, Z = 49.2, the variation range of velocity is from 0.04 m/s to 5.99 m/s. When Y = 2, Z = 50, the variation range of velocity is from 0.12 m/s to 6.39 m/s. When Y = 2, Z = 50.8, the variation range of velocity is from 0.03 m/s to 6.22 m/s. When Y = 2, Z = 51.6, the variation range of velocity is from 0.01 m/s to 2.44 m/s.

(ii)  The variation range of velocity in the cross passage is from 0.01 m/s to 6.39 m/s. The velocity is high speed-based, and the changes of velocity are great. Overall, the velocity increases with the increase of X. The velocity keeps unchanged when the variation range of X is from -12 to -7, while the velocity increases rapidly when the variation range of X is from -7 to 12. It also can be concluded, the velocity in the center of the section is the maximum, and then it decreases gradually toward both sides of the section, i.e., the velocity is the maximum when Z = 50, while the velocity is the minimum when Z = 48.4 or 51.6.

(iii) Fig. 32(b) shows that, when Y = 2, Z = 48.4, the variation range of pressure is from 0.06 Pa to 51.1 Pa. When Y = 2, Z = 49.2, the variation range of pressure is from 0.80 Pa to 51.1 Pa. When Y = 2, Z = 50, the variation range of pressure is from 0.95 Pa to 51.1 Pa. When Y = 2, Z = 50.8, the variation range of pressure is from 0.77 Pa to 51.1 Pa. When Y = 2, Z = 51.6, the variation range of pressure is from -0.30 Pa to 51.1 Pa.

(iv)  In general, the pressure decreases continually with the increase of X. The pressure keeps at about 51 Pa when the variation range of X is from -12 to -7. The pressure decreases rapidly when the variation range of X is from -7 to 7. The pressure keeps at about 1 Pa when the variation range of X is from 7 to 12. In addition, the pressure curves of five probing lines are in good agreement, which shows that, in the width direction of the cross passage (Z-direction), the pressure values along the length direction (X-direction) of the cross passage are fixed.

(2)   As for the five probing lines in the left tunnel (Fig. 7(a)), their velocity curves and pressure curves are shown in Fig. 33.

It can be obtained from Fig. 33:

(i)   Fig. 33(a) shows that, when X = -14, Y = 2, the variation range of velocity is from 0 m/s to 0.037 m/s. When X = -16, Y = 2, the variation range of velocity is from 0 m/s to 0.027 m/s. When X = -18, Y = 2, the variation range of velocity is from 0 m/s to 0.024 m/s. When X = -20, Y = 2, the variation range of velocity is from 0 m/s to 0.020 m/s. When X = -22, Y = 2, the variation range of velocity is from 0 m/s to 0.019 m/s.

(ii)  In the process of flowing from the cross passage to the left tunnel, the velocity reduces obviously. The variation range of velocity in the left tunnel is from 0 m/s to 0.037 m/s, and the velocity is low speed-based. Overall, the velocity firstly increases and then decreases with the increase of Z. The velocity at the two working face is 0 m/s, and the velocity near by the cross passage is larger, i.e., the velocity is the minimum when Z = 0 or 100, while the velocity is the maximum when Z = 47.4. It also can be concluded, among the five selected probing lines, the velocity is the minimum when X = -22.

(iii) Fig. 33(b) shows that, when X = -14, Y = 2, the pressure keeps at 51.1 Pa unchanged. When X = -16, Y = 2, the pressure keeps at 51.1 Pa unchanged. When X = -18, Y = 2, the pressure keeps at 51.1 Pa unchanged. When X = -20, Y = 2, the pressure keeps at 51.1 Pa

(a) Velocity curves



(b) Pressure curves

Fig. 33 The velocity and pressure curves of the left tunnel

unchanged. When X = -22, Y = 2, the pressure keeps at 51.1 Pa unchanged.

(iv) In general, the pressure keeps at 51.1 Pa unchanged in the left tunnel. The pressure curves of five probing lines are in good agreement, which shows that, in the width direction of the left tunnel (X-direction), the pressure values along the length direction (Z-direction) of the left tunnel are fixed.

(3) As for the five probing lines in the right tunnel (Fig. 7(c)), their velocity curves and pressure curves are shown in Fig. 34.

It can be obtained from Fig. 34:

(i) Fig. 34(a) shows that, when X = 14, Y = 2, the variation range of velocity is from 0 m/s to 2.81 m/s. When X = 16, Y = 2, the variation range of velocity is from 0 m/s to 3.60 m/s. When X = 18, Y = 2, the variation range of velocity is from 0 m/s to 3.75 m/s. When X = 20, Y = 2, the variation range of velocity is from 0 m/s to 3.79 m/s. When X = 22, Y = 2, the variation range of velocity is from 0 m/s to 2.95 m/s.

(ii) In the process of flowing from the cross passage to the right tunnel, the velocity reduces obviously. The variation range of velocity in the right tunnel is from 0 m/s to 3.79 m/s, and the velocity is low speed-based. Overall, the velocity firstly increases and then decreases with the increase of Z. The velocity at the working face is 0 m/s, and the velocity near by

(a) Velocity curves
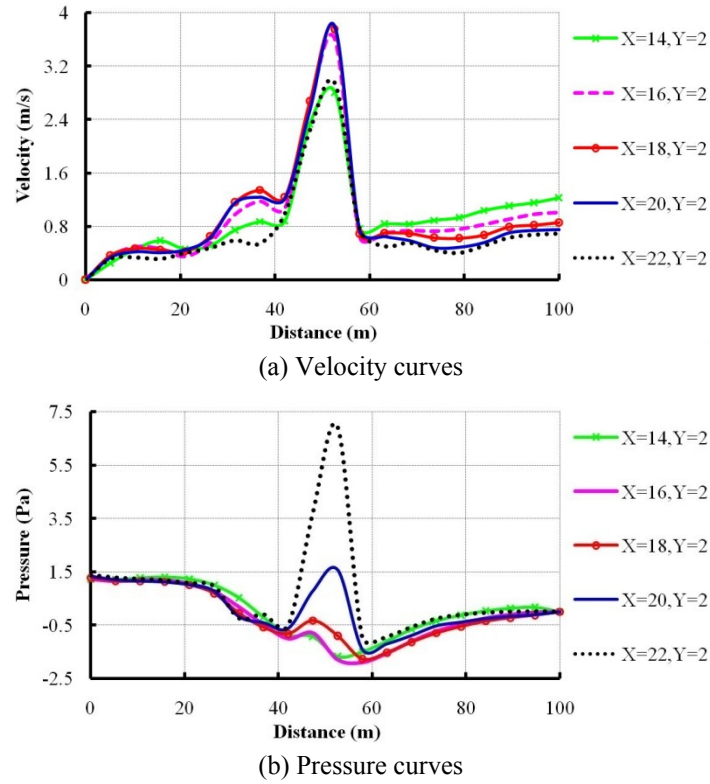


(b) Pressure curves

Fig. 34 The velocity and pressure curves of the right tunnel

      the cross passage is larger, i.e., the velocity is the minimum when $Z = 0$, while the velocity is the maximum when $Z = 52.6$. In addition, it also can be concluded, among the five selected probing lines, the velocity is the minimum when $X = 22$.

(iii) Fig. 34(b) shows that, when $X = 14$, $Y = 2$, the variation range of pressure is from -1.68 Pa to 1.31 Pa. When $X = 16$, $Y = 2$, the variation range of pressure is from -1.89 Pa to 1.23 Pa. When $X = 18$, $Y = 2$, the variation range of pressure is from -1.77 Pa to 1.28 Pa. When $X = 20$, $Y = 2$, the variation range of pressure is from -1.41 Pa to 1.34 Pa. When $X = 22$, $Y = 2$, the variation range of pressure is from -0.98 Pa to 6.92 Pa.

(iv) In the process of flowing from the cross passage to the right tunnel, the pressure reduces obviously. The variation range of pressure in the right tunnel is from -1.89 Pa to 6.92 Pa, and the pressure is low pressure-based. When the variation range of Z is from 0 to 40, the pressure gradually decreases. When the variation range of Z is from 40 to 60, the pressure first increases and then decreases. The pressure close to one side of the cross passage is the minimum, and then it increases gradually towards the other side, i.e., the pressure is the minimum when $X = 14$, while the pressure is the maximum when $X = 22$. When the variation range of Z is from 60 to 100, the pressure increases gradually, and it becomes 0 Pa at the right tunnel entrance (Outlet). Moreover, the pressure in the center of the section is the minimum, and then it increases gradually toward both sides of the section. In general, the pressure changes greatly in the vicinity of the cross passage, while it changes gently in other areas.

(a) Velocity curves
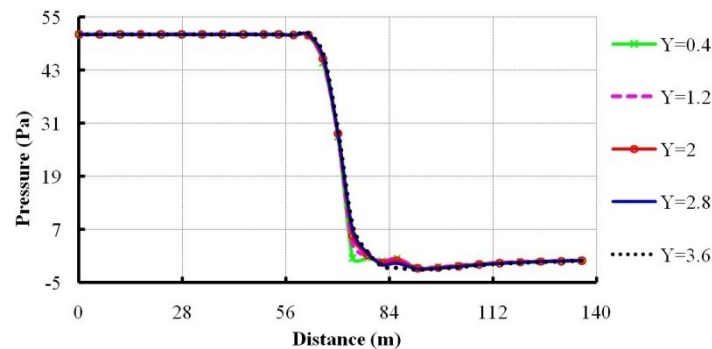


(b) Pressure curves

Fig. 35 The velocity and pressure curves of Y-direction

(4)  As for the five probing broken lines along the height direction (Y-direction) of the tunnel centerline (Fig. 7(d)), their velocity curves and pressure curves are shown in Fig. 35.

It can be obtained from Fig. 35:

(i)  Fig. 35(a) shows that, when Y = 0.4, the variation range of velocity is from 0 m/s to 2.14 m/s. When Y = 1.2, the variation range of velocity is from 0 m/s to 5.31 m/s. When Y = 2, the variation range of velocity is from 0 m/s to 6.38 m/s. When Y = 2.8, the variation range of velocity is from 0 m/s to 7.10 m/s. When Y = 3.6, the variation range of velocity is from 0 m/s to 5.84 m/s.

(ii)  In the cross passage, the velocity first increases and then decreases, and the velocity reaches its maximum value near by the water inrush position. Moreover, among the five selected probing lines, the velocity is the minimum when Y = 0.4. In the process of flowing from the cross passage to the left tunnel, the velocity reduces sharply. The velocity is about 0 m/s in the left tunnel. In the process of flowing from the cross passage to the right tunnel, the velocity decreases quickly. Then it changes gently in the right tunnel, and the velocity is low speed-based. Moreover, among the five selected probing lines, the velocity is the minimum when Y = 0.4 or 3.6.

(iii)  Fig. 35(b) shows that, when Y = 0.4, the variation range of pressure is from -1.59 Pa to 51.1 Pa. When Y = 1.2, the variation range of pressure is from -1.63 Pa to 51.1 Pa. When

Y = 2, the variation range of pressure is from -1.75 Pa to 51.1 Pa. When Y = 2.8, the variation range of pressure is from -1.91 Pa to 51.1 Pa. When Y = 3.6, the variation range of pressure is from -2.03 Pa to 51.1 Pa.

(iv) In general, the pressure decreases gradually with the increase of the distance to the left tunnel working face (away from the left tunnel entrance). The pressure keeps at 51.1 Pa in the left tunnel. The pressure decreases sharply in the cross passage, while it changes gently in the right tunnel, and it is close to 0 Pa at the right tunnel entrance (Outlet). In addition, the pressure curves of five probing broken lines coincide well, which shows that, in the height direction of the tunnels (Y-direction), the pressure values along the length direction of the tunnels are basically fixed.

### 4.4.3 The optimized escape routes

(1) According to the results of velocity curves, the velocity in the center of the section is the maximum, while it at boundaries is the minimum. Therefore, tunnel constructors should first move to the tunnel side wall and then escape quickly when water inrush happens.

(2) According to the results of pressure curves, the pressure change at the intersection area of the cross passage and the tunnels is large. So, tunnel constructors must not stay here for a short time when escaping.

(3) Water inrush from floor occurs in the middle position of the cross passage, i.e., Fig. 29(d). During the escaping, tunnel constructors in the cross passage should first move to the side wall and then pass through the cross passage rapidly, turn to the right tunnel and run to the entrance.

(4) Water inrush from floor occurs in the middle position of the cross passage, i.e., Fig. 29(d). During the escaping, tunnel constructors in the left tunnel should first move to the tunnel side wall and then pass through the cross passage quickly, and run to the right tunnel entrance.

(5) Water inrush from floor occurs in the middle position of the cross passage, i.e., Fig. 29(d). During the escaping, tunnel constructors in the right tunnel should first move to the tunnel side wall and then run to the right tunnel entrance.
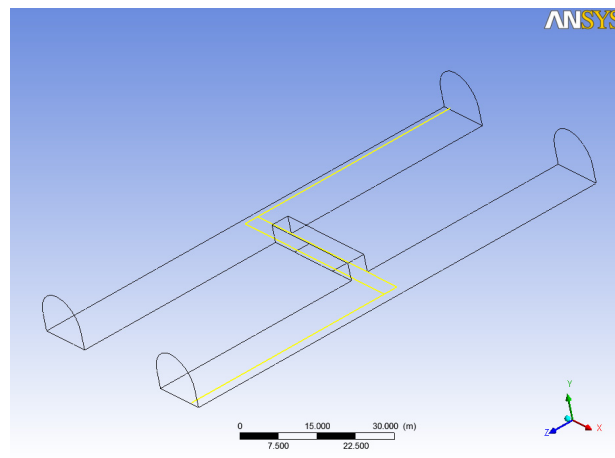


Fig. 36 The optimized escape routes (Case 4)

(6)     Water inrush from floor occurs in the middle position of the cross passage, i.e., Fig. 29(d). The velocity near by the working faces of the left and right tunnels is 0 m/s. Thus, if there is not enough time to escape, tunnel constructors can run to the trolley and other equipment in the vicinity of the working face (the left tunnel or the right tunnel).

Combined with this case, the optimized escape routes are shown in Fig. 36.

### 4.5 Case study 5

The excavation situation of this case is identical with case 3. During the left tunnel excavation, water inrush from floor occurs in the bottom of the working face (close to the left tunnel entrance), i.e., the floor below the left tunnel working face is the inlet of water inrush (velocity, 2 m/s), and the right tunnel entrance is the outlet of water inrush (pressure, 0 Pa). The scope of water inrush along the length direction of the left tunnel (Z-direction) is 4 m, and the width direction of the left tunnel (X-direction) is 12 m. The total area of water inrush is 48 m$^2$. As shown in Fig. 37, E is the water inrush position.
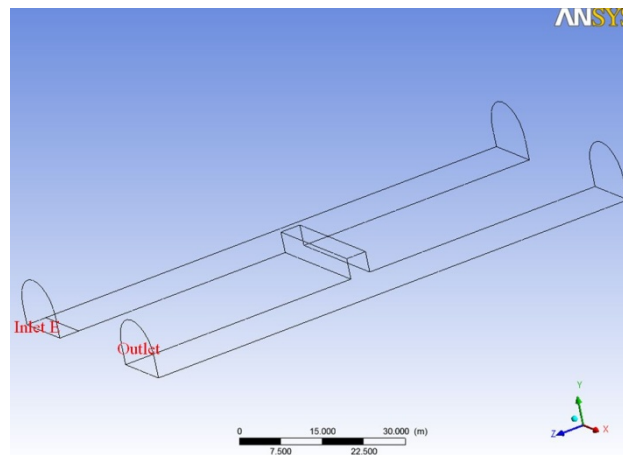


Fig. 37 The water inrush position in the left tunnel (Case 5)
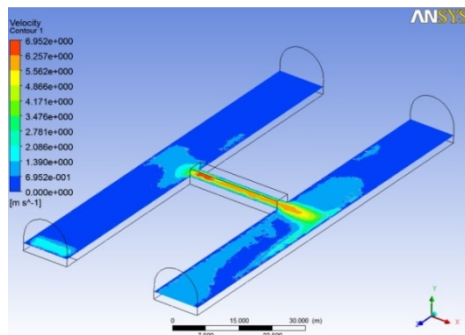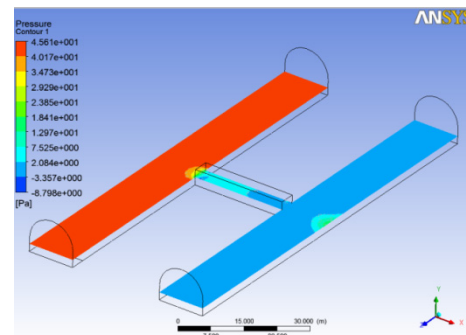


(a) Velocity contour                                    (b) Pressure contour

Fig. 38 Y = 2 section
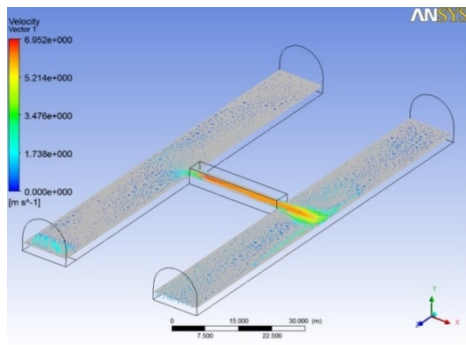
(c) Velocity vector
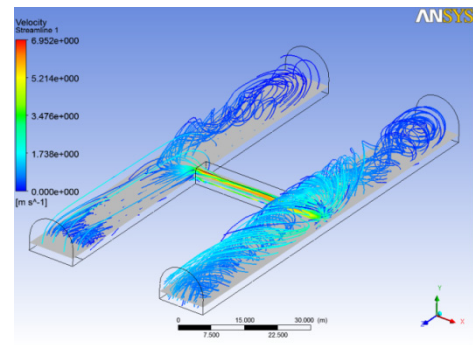


(d) Velocity streamline

Fig. 38 Continued
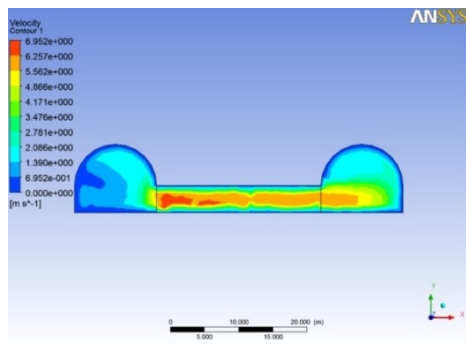


(a) Velocity contour
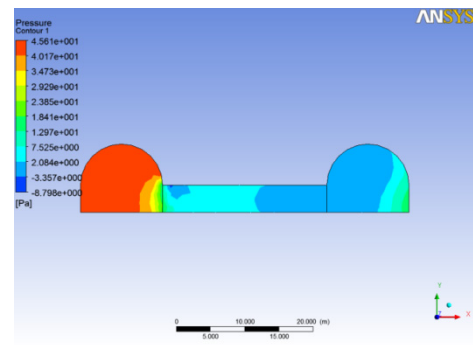


(b) Pressure contour
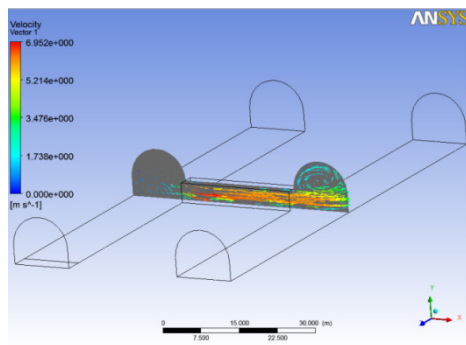


(c) Velocity vector
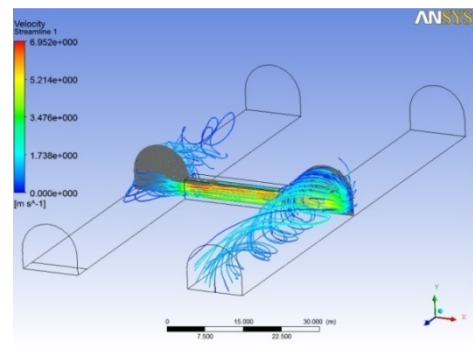


(d) Velocity streamline

Fig. 39 Z = 50 section

### 4.5.1 Simulated results

Y = 2 section and Z = 50 section are selected as examples. The calculation results are shown in Figs. 38 and 39.

### 4.5.2 Analysis

In order to shows the changes of velocity and pressure in the tunnels more vividly, a series of

probing lines are selected. The probing lines of the left tunnel, the cross passage and the right tunnel (Y = 2 section) are identical with the case study 1. The details of the above probing lines are shown in Table 1, and the corresponding figures are shown in Figs. 7(a), (b) and (c). As for five probing broken lines along the height direction (Y-direction) of the tunnel centerline, the details are shown in Table 2 and Fig. 40. All probing lines are researched and analyzed.

(1)  As for the five probing lines in the left tunnel (Fig. 7(a)), their velocity curves and pressure curves are shown in Fig. 41.

Table 2 The details of five probing broken lines

| The section | The location | The selected probing lines | The selected points | The figure |
|---|---|---|---|---|
| X = -18 | The left tunnel | X = -18, Y = 0.4, Z = 100~50 | 10 | |
| | | X = -18, Y = 1.2, Z = 100~50 | 10 | |
| | | X = -18, Y = 2.0, Z = 100~50 | 10 | |
| | | X = -18, Y = 2.8, Z = 100~50 | 10 | |
| | | X = -18, Y = 3.6, Z = 100~50 | 10 | |
| Z = 50 | The cross passage | Y = 0.4, Z = 50, X = -18~18 | 10 | Fig. 40 |
| | | Y = 1.2, Z = 50, X = -18~18 | 10 | |
| | | Y = 2.0, Z = 50, X = -18~18 | 10 | |
| | | Y = 2.8, Z = 50,X = -18~18 | 10 | |
| | | Y = 3.6, Z = 50, X = -18~18 | 10 | |
| X = 18 | The right tunnel | X = 18, Y = 0.4, Z = 50~100 | 10 | |
| | | X = 18, Y = 1.2, Z = 50~100 | 10 | |
| | | X = 18, Y = 2.0, Z = 50~100 | 10 | |
| | | X = 18, Y = 2.8, Z = 50~100 | 10 | |
| | | X = 18, Y = 3.6, Z = 50~100 | 10 | |



Fig. 40 The location of five probing broken lines

(a) Velocity curves
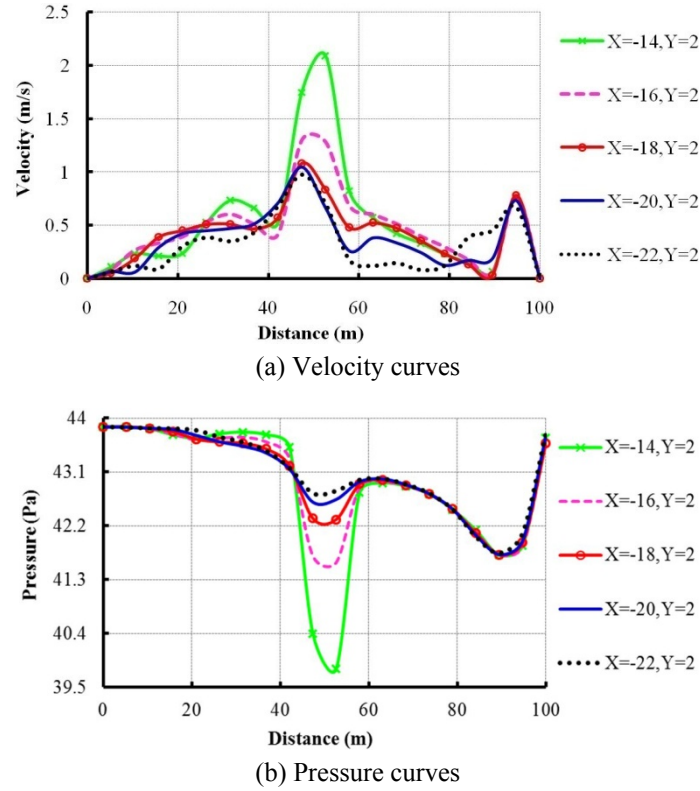


(b) Pressure curves

Fig. 41 The velocity and pressure curves of the left tunnel

It can be obtained from Fig. 41:

(i)   Fig. 41(a) shows that, when X = -14, Y = 2, the variation range of velocity is from 0 m/s to 2.09 m/s. When X = -16, Y = 2, the variation range of velocity is from 0 m/s to 1.30 m/s. When X = -18, Y = 2, the variation range of velocity is from 0 m/s to 1.08 m/s. When X = -20, Y = 2, the variation range of velocity is from 0 m/s to 1.05 m/s. When X = -22, Y = 2, the variation range of velocity is from 0 m/s to 0.97 m/s.

(ii)  Overall, the variation range of velocity in the left tunnel is from 0 m/s to 2.09 m/s. The velocity changes greatly, and it varies in a wave shape. The velocity in the vicinity of the cross passage is larger, then it decreases gradually toward both ends of the left tunnel, and it deduces to 0 m/s at the two working faces. In addition, the velocity close to one side of the cross passage is the maximum, and then it decreases gradually toward the other side, i.e., the velocity is the maximum when X = -14, while the velocity is the minimum when X = -22.

(iii) Fig. 41(b) shows that, when X = -14, Y = 2, the variation range of pressure is from 39.8 Pa to 43.9 Pa. When X = -16, Y = 2, the variation range of pressure is from 41.6 Pa to 43.9 Pa. When X = -18, Y = 2, the variation range of pressure is from 41.7 Pa to 43.9 Pa. When X = -20, Y = 2, the variation range of pressure is from 41.7 Pa to 43.9 Pa. When X = -22, Y = 2, the variation range of pressure is from 41.7 Pa to 43.9 Pa. The maximum pressure keeps unchanged at 43.9 Pa.

(iv) In general, the variation range of pressure in the left tunnel is from 39.8 Pa to 43.9 Pa. The pressure changes greatly, and it varies in a wave shape. Starting at the water inrush position (Z=100), the pressure first decreases and then increases. The pressure decreases rapidly and then increases rapidly near by the cross passage (Z=40~60). Later on, the pressure increases gradually, and it reaches its maximum value at the working face (Z=0). In addition, when the variation range of Z is from 40 to 60, the pressure close to one side of the cross passage is the minimum, and then it increases gradually toward the other side, i.e., the pressure is the minimum when X = -14, while the pressure is the maximum when X = -22. When the variation range of Z is from 60 to 100, the pressure curves of five probing lines are in good agreement.

(2) As for the five probing lines in the cross passage (Fig. 7(b)), their velocity curves and pressure curves are shown in Fig. 42.

It can be obtained from Fig. 42:

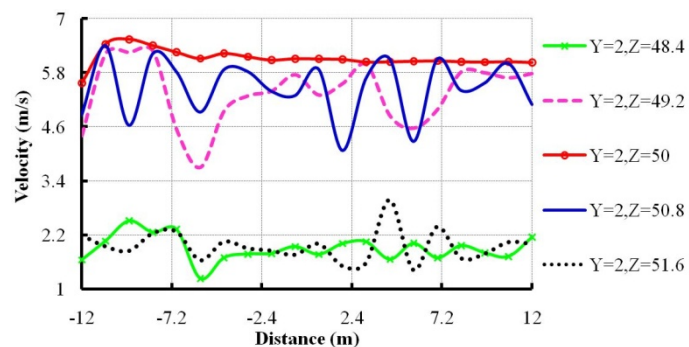(i) Fig. 42(a) shows that, when Y = 2, Z = 48.4, the variation range of velocity is from 1.23 m/s to 2.51 m/s. When Y = 2, Z = 49.2, the variation range of velocity is from 3.70 m/s to 6.28 m/s. When Y = 2, Z = 50, the variation range of velocity is from 5.56 m/s to 6.54 m/s. When Y = 2, Z = 50.8, the variation range of velocity is from 4.07 m/s to 6.40 m/s. When Y = 2, Z = 51.6, the variation range of velocity is from 1.43 m/s to 2.98 m/s.



(a) Velocity curves
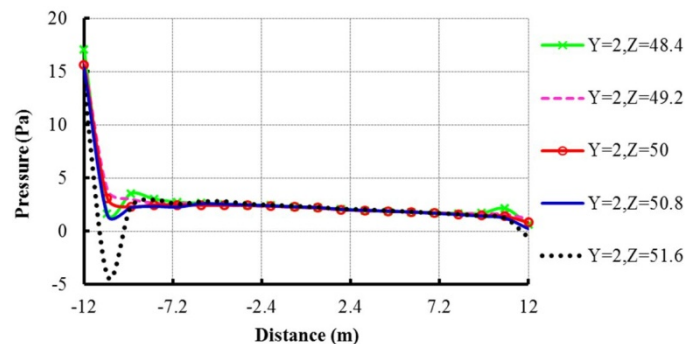


(b) Pressure curves

Fig. 42 The velocity and pressure curves of the cross passage

(ii)   In the process of flowing from the left tunnel to the cross passage, the velocity increases obviously. The variation range of velocity in the cross passage is from 1.23 m/s to 6.54 m/s, and the velocity is high speed-based. In addition, it also can be concluded, the velocity in the center of the section is the maximum, and then it decreases gradually toward both sides of the section, i.e., the velocity is the maximum when $Z = 50$, while it is the minimum when $Z = 48.4$ or $51.6$.

(iii)  Fig. 42(b) shows that, when $Y = 2$, $Z = 48.4$, the variation range of pressure is from 0.63 Pa to 17.0 Pa. When $Y = 2$, $Z = 49.2$, the variation range of pressure is from 1.17 Pa to 16.0 Pa. When $Y = 2$, $Z = 50$, the variation range of pressure is from 0.83 Pa to 15.6 Pa. When $Y = 2$, $Z = 50.8$, the variation range of pressure is from 0.24 Pa to 15.4 Pa. When $Y = 2$, $Z = 51.6$, the variation range of pressure is from -4.16 Pa to 13.7 Pa.

(iv)   In the process of flowing from the left tunnel to the cross passage, the pressure decreases rapidly. The variation range of pressure in the cross passage is from -4.16 Pa to 17.0 Pa. On the whole, the pressure is the maximum at the starting point of the cross passage, and then it decreases gradually with the increase of X. When the variation range of X is from -12 to -9, the pressure decreases sharply, and the pressure is the minimum when $Z = 51.6$. When the variation range of X is from -9 to 12, the pressure decreases slowly, and the pressure curves of five probing lines coincide well.

(3)    As for the five probing lines in the right tunnel (Fig. 7(c)), their velocity curves and pressure curves are shown in Fig. 43.

It can be obtained from Fig. 43:

(i)    Fig. 43(a) shows that, when $X = 14$, $Y = 2$, the variation range of velocity is from 0 m/s to 2.72 m/s. When $X = 16$, $Y = 2$, the variation range of velocity is from 0 m/s to 3.43 m/s. When $X = 18$, $Y = 2$, the variation range of velocity is from 0 m/s to 3.67 m/s. When $X = 20$, $Y = 2$, the variation range of velocity is from 0 m/s to 3.58 m/s. When $X = 22$, $Y = 2$, the variation range of velocity is from 0 m/s to 3.00 m/s.

(ii)   In the process of flowing from the cross passage to the right tunnel, the velocity reduces obviously. The variation range of velocity in the right tunnel is from 0 m/s to 3.67 m/s. On the whole, the velocity firstly increases and then decreases with the increase of Z. The velocity at the working face is 0 m/s, and it is higher in the vicinity of the cross passage, i.e., the velocity is the minimum when $Z = 0$, while it is the maximum when $Z = 50$. In addition, it also can be concluded, among the five selected probing lines, the velocity is the minimum when $X = 22$.

(iii)  Fig. 43(b) shows that, when $X = 14$, $Y = 2$, the variation range of pressure is from -1.88 Pa to 1.23 Pa. When $X = 16$, $Y = 2$, the variation range of pressure is from -1.82 Pa to 1.14 Pa. When $X = 18$, $Y = 2$, the variation range of pressure is from -1.62 Pa to 1.19 Pa. When $X = 20$, $Y = 2$, the variation range of pressure is from -1.34 Pa to 1.27 Pa. When $X = 22$, $Y = 2$, the variation range of pressure is from -1.03 Pa to 6.33 Pa.
       In the process of flowing from the cross passage to the right tunnel, the pressure reduces obviously. The variation range of pressure in the right tunnel is from -1.88 Pa to 6.33 Pa. When the variation range of Z is from 0 to 40, the pressure gradually decreases. The pressure in the center of the section is the minimum, and then it increases gradually toward both sides of the section. When the variation range of Z is from 40 to 60, the pressure first increases and then decreases. The pressure is the maximum when $X = 22$, while it is the

(a) Velocity curves
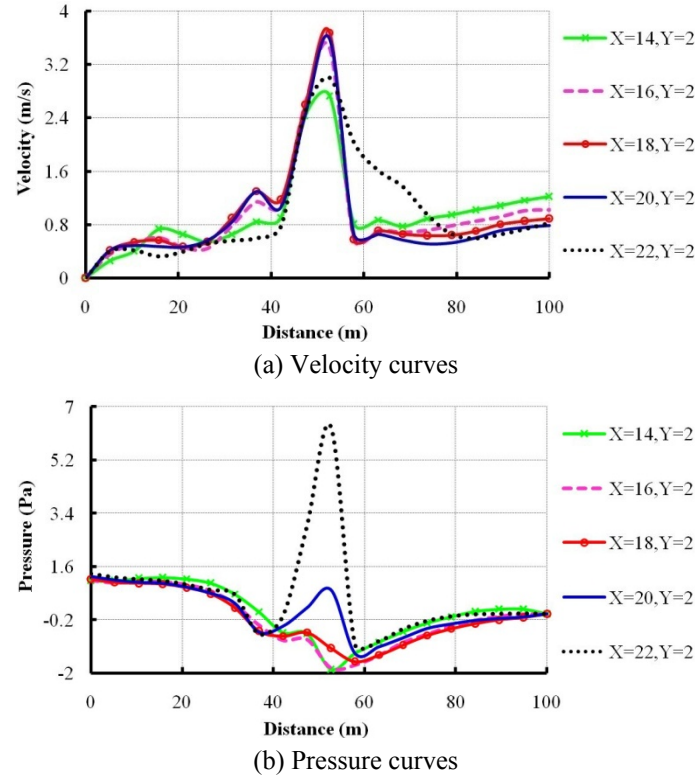


(b) Pressure curves

Fig. 43 The velocity and pressure curves of the right tunnel

minimum when X = 14. When the variation range of Z is from 60 to 100, the pressure increases gradually and it becomes 0 Pa at the right tunnel entrance (Outlet). Moreover, the pressure in the center of the section is the minimum, and then it increases gradually toward both sides of the section. On the whole, the pressure changes greatly in the vicinity of the cross passage, while it changes gently in other areas.

(4) As for the five probing broken lines along the height direction (Y-direction) of the tunnel centerline (Fig. 40), their velocity curves and pressure curves are shown in Fig. 44.

It can be obtained from Fig. 44:

(i) Fig. 44(a) shows that, when Y = 0.4, the variation range of velocity is from 0 m/s to 2.32 m/s. When Y = 1.2, the variation range of velocity is from 0 m/s to 6.63 m/s. When Y = 2, the variation range of velocity is from 0 m/s to 6.69 m/s. When Y = 2.8, the variation range of velocity is from 0 m/s to 6.10 m/s. When Y = 3.6, the variation range of velocity is from 0 m/s to 4.71 m/s.

(ii) The velocity changes gently in the left tunnel, and the velocity is the minimum when Y = 0.4. In the process of flowing from the left tunnel to the cross passage, the velocity increases obviously. In the cross passage, the velocity in the center of the section is the maximum, and then it decreases gradually toward the upper and lower, i.e., the velocity is the maximum when Y = 2, while it is the minimum when Y = 0.4 or 3.6. In the process

(a) Velocity curves
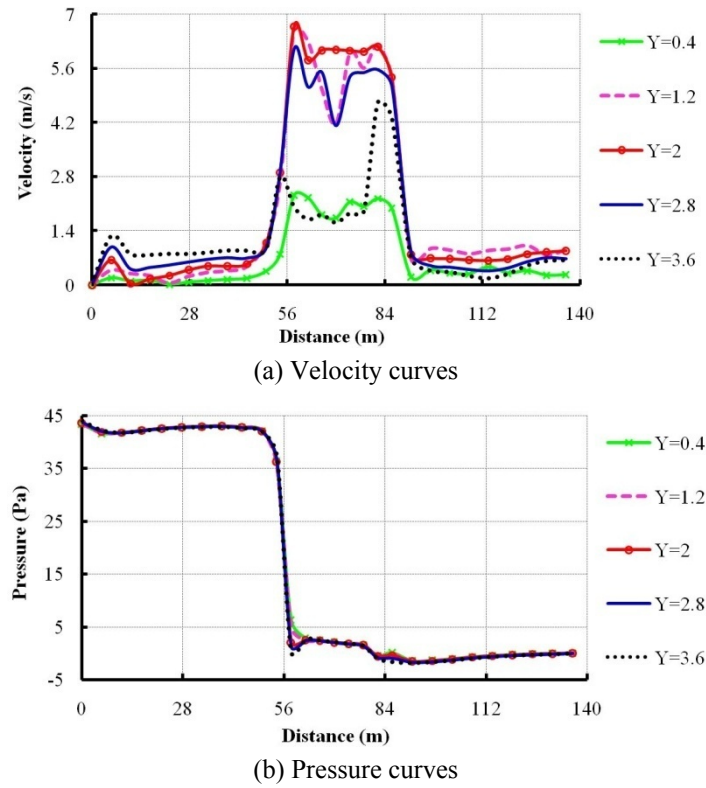


(b) Pressure curves

Fig. 44 The velocity and pressure curves of Y-direction

of flowing from the cross passage to the right tunnel, the velocity decreases rapidly. The velocity changes more gently in the right tunnel, and the velocity is lower When Y = 0.4 or 3.6.

(iii) Fig. 44(b) shows that, when Y = 0.4, the variation range of pressure is from -1.47 Pa to 43.4 Pa. When Y = 1.2, the variation range of pressure is from -1.52 Pa to 43.5 Pa. When Y = 2, the variation range of pressure is from -1.59 Pa to 43.6 Pa. When Y = 2.8, the variation range of pressure is from -1.68 Pa to 43.8 Pa. When Y = 3.6, the variation range of pressure is from -1.64 Pa to 44.1 Pa.

(iv) The pressure changes gently in the left tunnel. In the process of flowing from the left tunnel to the cross passage, the pressure reduces sharply. Then, in the process of flowing from the cross passage to the right tunnel, the pressure continues to reduce slowly. On the whole, the pressure near by the water inrush position is the maximum, and then it decreases gradually with the increase of the distance. In addition, the pressure curves of five probing lines are in good agreement, which shows that, in the height direction of the tunnels (Y-direction), the pressure values along the length direction of the tunnels are fixed.

### 4.5.3 The optimized escape routes

(1) According to the results of velocity curves, the velocity in the center of the section is the maximum, while it at boundaries is the minimum. Therefore, tunnel constructors should first move to the tunnel side wall and then escape quickly when water inrush happens.
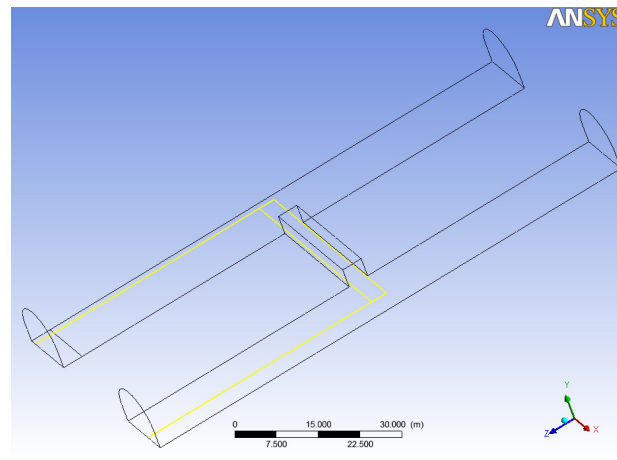
Fig. 45 The optimized escape routes (Case 5)

(2) According to the results of pressure curves, the pressure change at the intersection area of the cross passage and the tunnels is large. So, tunnel constructors must not stay here for a short time when escaping.

(3) Water inrush from floor occurs in the bottom of the left tunnel working face, i.e., Fig. 37(E). During the escaping, tunnel constructors in the left tunnel should pass through the cross passage rapidly, turn to the right tunnel and run to the entrance.

(4) Water inrush from floor occurs in the bottom of the left tunnel working face, i.e., Fig. 37(E). The velocity near by the left tunnel working face (away from the left tunnel entrance) is small. Thus, if there is not enough time to escape, tunnel constructors can run to the trolley and other equipment in the vicinity of the left tunnel working face (away from the left tunnel entrance).

(5) Water inrush from floor occurs in the bottom of the left tunnel working face, i.e., Fig. 37(E). The velocity nearby the right tunnel working face is 0 m/s. Thus, if there is not enough time to escape, tunnel constructors can run to the trolley and other equipment in the vicinity of the right tunnel working face.

(6) Water inrush from floor occurs in the bottom of the left tunnel working face, i.e., Fig. 37(E). The velocity and pressure on the high location of the cross passage are both small, so some rescuing equipment can be set up there.

Combined with this case, the optimized escape routes are shown in Fig. 45.


## 5. Results comparison and discussion

In order to compare the water flow characteristics under the conditions of the same water inrush position and different excavation situations, case study 1 and case study 3, case study 2 and case study 4 are compared and discussed respectively. In order to compare the water flow characteristics under the conditions of the same excavation situation and different water inrush positions, case study 1 and case study 2, case study 3, case study 4 and case study 5 are compared and discussed respectively.

## *5.1 Different excavation situations*

### *5.1.1 Case study 1 and case study 3*

The water inrush position of case study 1 and case study 3 is the same, i.e., the floor in the bottom of the left tunnel working face, which is shown in Figs. 4(a) and 21(c), and the water inrush areas are also identical. But both excavation situations are different, which results in different boundary condition setting, i.e., for case study 1, the left and right tunnel entrances are pressure outlet boundaries simultaneously, while for case study 3, only the right tunnel entrance is a pressure outlet boundary. The water flow characteristics after inrushing can be discussed and summarized by comparing the corresponding velocity and pressure curves under the two case studies.

(1) In the left tunnel, compare Figs. 8(a) and 24(a), the following conclusions can be drawn. The velocity change near by the water inrush position is the same in two excavation situations, i.e., the velocity first increases and then decreases. Later, when the left and right tunnel entrances are pressure outlet boundaries simultaneously, the velocity increases continually, and it reaches its maximum value at the left tunnel entrance. While only the right tunnel entrance is a pressure outlet boundary, the velocity varies in a wave shape, and it reaches its maximum value in the vicinity of the cross passage. Then, the velocity decreases continually, and it reduces to 0 m/s at the left tunnel working face (close to the left tunnel entrance). Moreover, compared with the former, the velocity change of the latter is larger. In addition, as for the former excavation situation, the velocity is the minimum when X = -14 or -22. As for the latter excavation situation, the velocity is the minimum when X = -22.

(2) In the left tunnel, compare Fig. 8(b) and Fig. 24(b), the following conclusions can be drawn. In two excavation situations, the pressure first decreases and then increases. Moreover, when the left and right tunnel entrances are pressure outlet boundaries simultaneously, the variation range of pressure is from -1.49 Pa to 0.534 Pa, and the value is smaller. When only the right tunnel entrance is a pressure outlet boundary, the variation range of pressure is from 39.2 Pa to 44.6 Pa, and the value is obviously larger. In addition, for the former, the pressure changes greatly in the vicinity of the water inrush position. For the latter, the pressure changes greatly near by the water inrush position and the cross passage.

(3) In the cross passage, compare Figs. 9(a) and 25(a), the following conclusions can be drawn. The variation trend of the pressure is basically the same in two excavation situations. When the left and right tunnel entrances are pressure outlet boundaries simultaneously, the variation range of velocity is from 0.03 m/s to 0.253 m/s, and the value is smaller. While only the right tunnel entrance is a pressure outlet boundary, the variation range of velocity is from 1.30 m/s to 6.49 m/s, and the value is obviously larger. In addition, when Z = 51.6, the velocity is the minimum in two excavation situations.

(4) In the cross passage, compare Figs. 9(b) and 25(b), the following conclusions can be drawn. When the left and right tunnel entrances are pressure outlet boundaries simultaneously, the pressure increases gradually. While only the right tunnel entrance is a pressure outlet boundary, the pressure decreases gradually. As for the former, the variation range of pressure is from -0.096 Pa to -0.013 Pa, and the value is smaller. As for the latter, the variation range of pressure is from -2.90 Pa to 16.9 Pa, and the value is obviously larger.

(5)  In the right tunnel, compare Figs. 10(a) and 26(a), the following conclusions can be drawn. In two excavation situations, the velocity is 0 m/s at the working face, then, on the whole, the velocity shows an increased tendency, and it changes greatly in the vicinity of the cross passage. Moreover, when the left and right tunnel entrances are pressure outlet boundaries simultaneously, the variation range of velocity is from 0 m/s to 0.053 m/s, and the value is smaller. While only the right tunnel entrance is a pressure outlet boundary, the variation range of velocity is from 0 m/s to 3.73 m/s, and the value is obviously larger. In addition, when X = 22, the velocity is the minimum in two excavation situations.

(6)  In the right tunnel, compare Figs. 10(b) and 26(b), the following conclusions can be drawn. In two excavation situations, the pressure changes greatly in the vicinity of the cross passage, while it changes gently in other areas. When the left and right tunnel entrances are pressure outlet boundaries simultaneously, on the whole, the pressure has increase tendency. The variation range of pressure is from -0.0021 Pa to -0.0001 Pa, and the value is smaller. While only the right tunnel entrance is a pressure outlet boundary, on the whole, the pressure has decrease tendency. The variation range of pressure is from -1.74 Pa to 6.50 Pa, and the value is obviously larger.

(7)  In Y-direction, compare Figs. 11(a) and 27(a), the following conclusions can be drawn. In the left tunnel, the velocity change is basically the same in two excavation situations, and the velocity is the lowest when Y = 0.4. In the cross passage, when the left and right tunnel entrances are pressure outlet boundaries simultaneously, the velocity is lower and it changes gently. While only the right tunnel entrance is a pressure outlet boundary, the velocity is higher and it changes greatly. Moreover, when Y = 0.4 or 3.6, the velocity is the lowest in two excavation situations. In the right tunnel, as for the former, the velocity keeps unchanged. For the latter, the velocity changes gently, and it is the lowest when Y = 0.4 or 3.6.

(8)  In Y-direction, compare Figs. 11(b) and 27(b), the following conclusions can be drawn. When the left and right tunnel entrances are pressure outlet boundaries simultaneously, the pressure first decreases and then increases. While only the right tunnel entrance is a pressure outlet boundary, the pressure decreases gradually. As for the former, the pressure changes greatly in the vicinity of water inrush position. As for the latter, the pressure changes greatly on both ends of the cross passage. Moreover, the latter pressure is much larger than the former.

### 5.1.2 Case study 2 and case study 4

The water inrush position of case study 2 and case study 4 is the same, i.e., the floor in the middle position of the cross passage, which is shown in Figs. 13(b) and 29(d), and the water inrush areas are also identical. But both excavation situations are different, which results in different boundary condition setting, i.e., for case study 2, the left and right tunnel entrances are pressure outlet boundaries simultaneously, while for case study 4, only the right tunnel entrance is a pressure outlet boundary. The water flow characteristics after inrushing can be discussed and summarized by comparing the corresponding velocity and pressure curves under the two case studies.

(1)  In the cross passage, compare Figs. 16(a) and 32(a), the following conclusions can be drawn. The velocity change is completely different in two excavation situations. On the whole, when the left and right tunnel entrances are pressure outlet boundaries simultaneously, the velocity first decreases and then increases. While only the right tunnel

entrance is a pressure outlet boundary, the pressure increases gradually. Moreover, compared with the former, the velocity change of the latter is larger. In addition, as for the former, the velocity is the minimum when Z = 48.4, while for the latter, the velocity is the minimum when Z = 48.4 or 51.6.

(2)　In the cross passage, compare Figs. 16(b) and 32(b), the following conclusions can be drawn. The pressure change is completely different in two excavation situations. When the left and right tunnel entrances are pressure outlet boundaries simultaneously, the pressure first increases and then decreases, and it reaches its maximum value in the middle position of the cross passage. The variation range of pressure is from -0.10 Pa to 13.0 Pa. While only the right tunnel entrance is a pressure outlet boundary, the pressure is the maximum at the starting points of the cross passage, then it decreases gradually, and the variation range of pressure is from -0.30 Pa to 51.1 Pa. Compared with the former, the variation range of the latter is larger.

(3)　In the left tunnel, compare Figs. 17(a) and 33(a), the following conclusions can be drawn. In two excavation situations, the velocity first increases and then decreases. The velocity changes greatly in the vicinity of the cross passage, and it reaches its maximum value in the middle position. When the left and right tunnel entrances are pressure outlet boundaries simultaneously, the variation range of velocity is from 0 m/s to 1.99 m/s. While only the right tunnel entrance is a pressure outlet boundary, the variation range of velocity is from 0 m/s to 0.037 m/s. Compared with the former, the latter velocity is obviously smaller. In addition, when X = -22, the velocity is the minimum in two excavation situations.

(4)　In the left tunnel, compare Figs. 17(b) and 33(b), the following conclusions can be drawn. The pressure change is completely different in two excavation situations. When the left and right tunnel entrances are pressure outlet boundaries simultaneously, the variation range of pressure is from -0.49 Pa to 1.64 Pa, and the pressure changes greatly near by the cross passage. While only the right tunnel entrance is a pressure outlet boundary, the pressure keeps at 51.1 Pa unchanged. In addition, compared with the former, the latter pressure is obviously larger.

(5)　In the right tunnel, compare Figs. 18(a) and 34(a), the following conclusions can be drawn. In two excavation situations, the velocity first increases and then decreases. The velocity changes greatly in the vicinity of the cross passage, and it reaches its maximum value in the middle position. When the left and right tunnel entrances are pressure outlet boundaries simultaneously, the variation range of velocity is from 0 m/s to 1.92 m/s. While only the right tunnel entrance is a pressure outlet boundary, the variation range of velocity is from 0 m/s to 3.79 m/s. Compared with the former, the latter velocity is obviously larger. In addition, when X = 22, the velocity is the minimum in two excavation situations.

(6)　In the right tunnel, compare Figs. 18(b) and 34(b), the following conclusions can be drawn. In two excavation situations, the variation trend of the pressure is basically same, and the pressure changes greatly near by the cross passage. But when the left and right tunnel entrances are pressure outlet boundaries simultaneously, the variation range of pressure is from -0.49 Pa to 1.78 Pa. While only the right tunnel entrance is a pressure outlet boundary, the variation range of pressure is from -1.89 Pa to 6.92 Pa. Compared with the former, the latter pressure is larger.

(7)　In Y-direction, compare Figs. 19(a) and 35(a), the following conclusions can be drawn. In the left tunnel, when the left and right tunnel entrances are pressure outlet boundaries

simultaneously, the velocity increases gradually, and it is the lowest when Y = 0.4. While only the right tunnel entrance is a pressure outlet boundary, the velocity keeps at 0 m/s unchanged. In the cross passage, the velocity changes greatly in two excavation situations, and it is the lowest when Y = 0.4. In the right tunnel, the velocity changes gently in two excavation situations, and the velocity curves are basically the same, moreover, the velocity is the lowest when Y = 0.4 or 3.6.

(8)  In Y-direction, compare Figs. 19(b) and 35(b), the following conclusions can be drawn. The pressure changes greatly in the cross passage, and it changes gently in other areas. On the whole, when the left and right tunnel entrances are pressure outlet boundaries simultaneously, the pressure first increases and then decreases. While only the right tunnel entrance is a pressure outlet boundary, the pressure decreases gradually. Moreover, the latter pressure is much larger than the former.

### 5.2 Different water inrush positions

### 5.2.1 Case study 1 and case study 2

The excavation situation of case study 1 and case study 2 is the same, i.e., the left and right tunnel entrances are pressure outlet boundaries simultaneously, and the water inrush areas are also identical. But both water inrush positions are different, for case study 1, water inrush from floor occurs in the bottom of the left tunnel working face, which is shown in Fig. 4(a), while for case study 2, water inrush from floor occurs in the middle position of the cross passage, which is shown in Fig. 13(b). The water flow characteristics after inrushing can be discussed and summarized by comparing the corresponding velocity and pressure curves under the two case studies.

(1)  Compare Figs. 8(a), 9(a), 10(a), 11(a) and Figs. 16(a), 17(a), 18(a), 19(a), the following conclusions can be drawn. Under the conditions of the two water inrush positions, the velocity in the center of the section is the maximum, and then it decreases gradually toward both sides of the section. In addition, when water inrush from floor occurs in the bottom of the left tunnel working face, the velocity is the maximum in the left tunnel, followed by the cross passage, and it is the minimum in the right tunnel. In other words, the water flows to outside mainly through the left tunnel. When water inrush from floor occurs in the middle position of the cross passage, the velocity is relatively higher in the cross passage, and the velocity change is basically the same in the left and right tunnels. In other words, starting from water inrush position, the water mainly flows to both ends of the cross passage, and then turns to the left and right tunnels entrances.

(2)  Compare Figs. 8(b), 9(b), 10(b), 11(b) and Figs. 16(b), 17(b), 18(b), 19(b), the following conclusions can be drawn. Under the conditions of the two water inrush positions, the pressure at the intersection area of the cross passage and the tunnels is relatively larger. In addition, when water inrush from floor occurs in the bottom of the left tunnel working face, the pressure is the maximum in the left tunnel, followed by the cross passage, and it is the minimum in the right tunnel. When water inrush from floor occurs in the middle position of the cross passage, the pressure is relatively higher in the cross passage, and the pressure change is basically the same in the left and right tunnels.

### 5.2.2 Case study 3, case study 4 and case study 5

The excavation situation of case study 3, case study 4 and case study 5 is the same, i.e., only the right tunnel entrance is a pressure outlet boundary, and the water inrush areas are also identical.

But their water inrush positions are different, for case study 3, water inrush from floor occurs in the bottom of the left tunnel working face (away from the left tunnel entrance), which is shown in Fig. 21(c). For case study 4, water inrush from floor occurs in the middle position of the cross passage, which is shown in Fig. 29(d). And for case study 5, water inrush from floor occurs in the bottom of the left tunnel working face (close to the left tunnel entrance), which is shown in Fig. 37(e). The water flow characteristics after inrushing can be discussed and summarized by comparing the corresponding velocity and pressure curves under the three case studies.

(1) Compare Figs. 24(a), 25(a), 26(a), 27(a), Figs. 32(a), 33(a), 34(a), 35(a) and Figs. 41(a), 42(a), 43(a), 44(a), the following conclusions can be drawn. Under the conditions of three water inrush positions, the velocity is the maximum in the cross passage, followed by the right tunnel and it is the minimum in the left tunnel. Besides, the velocity greatly changes in the cross passage. Moreover, the velocity in the center of the section is the maximum, and then it decreases gradually toward both sides of the section. In addition, when water inrush from floor occurs in the bottom of the left tunnel working face, starting from the water inrush position, the water mainly flows to the cross passage, and then turns to the right tunnel entrance. When water inrush from floor occurs in the middle position of the cross passage, the water mainly flows to the right tunnel entrance through the cross passage.

(2) Compare Figs. 24(b), 25(b), 26(b), 27(b), Figs. 32(b), 33(b), 34(b), 35(b) and Figs. 41(b), 42(b), 43(b), 44(b), the following conclusions can be drawn. Under the conditions of the three water inrush positions, the pressure is the maximum in the left tunnel, followed by the cross passage, and it is the minimum in the right tunnel. Moreover, the pressure at the intersection area of the cross passage and the tunnels is relatively larger.

## 6. Conclusions

In the present study, the high risk karst tunnel, Qiyueshan tunnels are taken as the research background. The finite element model is built in the ANSYS Workbench. Numerical simulation is carried out by using the FLUENT software. Five case studies of water inrush from the tunnel floor are investigated during the tunnel excavation. The corresponding velocity contour, pressure contour, velocity vector and velocity streamline are obtained. In order to show the variation of velocity and pressure in the tunnels more clearly, a series of probing lines are selected in a plane. Then, the variation characteristics of velocity and pressure along with distance are analyzed. Finally, the optimized escape routes are obtained. Compared with these five case studies, the water flow characteristics after inrushing in process of the karst tunnels excavation are discussed and summarized. The following conclusions are reached:

(1) The velocity nearby the tunnel side wall is the minimum, while it is the maximum in the middle position. Therefore, tunnel constructors should first move to the tunnel side wall and then escape quickly when water inrush happens.

(2) The pressure change at the intersection area of the cross passage and tunnels is large. Thus, tunnel constructors must not stay here for a short while when escaping.

(3) When water inrush from the tunnel floor happens in the left tunnel, if tunnel constructors meet the cross passage during escaping, they should pass through it rapidly, turn to the right tunnel without water inrush and run to the entrance.

(4)    When water inrush from the tunnel floor happens in the left tunnel, the velocity and pressure nearby the right tunnel working face are both small. Thus, if there is not enough time to escape, tunnel constructors can run to the trolley and other equipment in the vicinity of the right tunnel working face.

(5)    When water inrush from the tunnel floor happens in the left tunnel, the velocity and pressure at the high location of the cross passage are both small, so some rescuing equipment can be set up there.

(6)    When water inrush from the tunnel floor happens in the cross passage, tunnel constructors should move to the side wall quickly, turn to the left or right tunnel and run to the entrance.

(7)    When water inrush from the tunnel floor happens in the cross passage, the velocity near by the working faces of the left and right tunnels is low. Thus, if there is not enough time to escape, tunnel constructors can run to the trolley and other equipment in the vicinity of the working face (the left tunnel or the right tunnel).

## Acknowledgments

## References

Chen, L.W., Zhang, S.L. and Gui, H.R. (2014), "Prevention of water and quicksand inrush during extracting contiguous coal seams under the lowermost aquifer in the unconsolidated Cenozoic alluvium — A case study", *Arab. J. Geosci*, **7**(6), 2139-2149.

Cho, J.W., Jeon, S., Jeong, H.Y. and Chang, S.H. (2013), "Evaluation of cutting efficiency during TBM disc cutter excavation within a Korean granitic rock using linear-cutting-machine testing and photogrammetric measurement", *Tunn. Undergr. Sp. Tech.*, **35**, 37-54.

Di, Q.Y., Wu, F.Q., Wang, G.J., Tao, B., Gong, F., An, Z.G., Shi, K.F., Li, Y.X., Wang, R. and Wang, M.Y. (2005), "Geophysical exploration over long deep tunnel for west route of south-to-north water transfer project", *Chinese J. Rock Mech. Eng.*, **24**(20), 3631-3638.

Do, N.A., Oreste, P., Dias, D., Antonello, C., Irini, D.M. and Livio, L. (2014), "Stress and strain state in the segmental linings during mechanized tunnelling", *Geomech. Eng., Int. J.*, **7**(1), 75-85.

Fahimifar, A., Ghadami, H. and Ahmadvand, M. (2015), "The ground response curve of underwater tunnels, excavated in a strain-softening rock mass", *Geomech. Eng, Int. J.*, **8**(3), 323-359.

Golob, R., Stokelj, T. and Grgic, D. (1998), "Neural-network-based water inflow forecasting", *Control Eng. Pract.*, **6**(5), 593-600.

Hu, Y., Yan, G. and Shi, X. (2008), "Study on physical and numerical simulation of water inrush prediction theory for coal mining above confined aquifer", *Chinese J. Rock Mech. Eng.*, **27**(1), 9-15.

Huang, C.H., Feng, T., Wang, W.J. and Liu, H. (2010), "Mine water inrush prediction based on fractal and support vector machines", *J. Chinese Coal Soc.*, **35**(5), 806-810.

Huang, H.F., Mao, X.B., Yao, B.H. and Pu, H. (2012), "Numerical simulation on fault water-inrush based on fluid-solid coupling theory", *J. Coal Sci. Eng.*, **18**(3), 291-296.

Islam, M.R. and Islam, M.S. (2005), "Water inrush hazard in Barapukuria coal mine, Dinajpur District,

Bangladesh", *Bangl. J. Geol.*, **24**(1), 1-17.

Ivars, D.M. (2006), "Water inflow into excavations in fractured rock — A three-dimensional hydro-mechanical numerical study", *Int. J. Rock Mech. Min. Sci.*, **43**(5), 705-725.

Jin, H., Shi, L.Q., Yu, X.G., Wei, J.C. and Li, S.C. (2009), "Mechanism of mine water-inrush through a fault from the floor", *Min. Sci. Tech*, **19**(3), 276-281.

Kong, H.L. and Chen, Z.Q. (2006), "Water-inrush-factor and its application in the analysis on harmfulness of water-inrush in the long wall mining in longgu coal mine", *J. Wuhan U. Tech.*, **28**(9), 80-81.

Kong, H.L., Miao, X.X., Wang, L.Z., Zhang, Y. and Chen, Z.Q. (2007), "Analysis of the harmfulness of water-inrush from coal seam floor based on seepage instability theory", *J. China U. Min. Tech.*, **17**(4), 453-458.

Lei, X., Zhang, J. and Xie, T. (2003), "Forecast for water-inrush from coal floor based on genetic neural networks", *Comput. Eng.*, **11**, 132-133.

Li, L.J. and Zhang, J.J. (1995), "Calculation and prediction of water-inrush from mining floor and its application", *Coal Geol. Explor.*, **23**(4), 34-38.

Li, L.J., Qian, M.G. and Li, S.G. (1996), "Mechanism of water-inrush through fault", *J. China Coal Soc.*, **21**(2), 119-123.

Li, S.C., Li, S.C., Zhang, Q.S., Xue, Y.G., Ding, W.T., Zhong, S.H., He, F.L. and Lin, Y.S. (2007), "Forecast of karst-fractured groundwater and defective geological conditions", *Chinese J. Rock Mech. Eng.*, **26**(2), 217-225.

Li, S.C., Xue, Y.G., Zhang, Q.S., Li, S.C., Li, L.P., Sun, K.G., Ge, Y.H., Su, M.X., Zhong, S.H. and Li, X. (2008), "Key technology study on comprehensive prediction and early-warning of geological hazards during construction in high-risk karst areas", *Chinese J. Rock Mech. Eng.*, **27**(7), 1297-1307.

Li, L.C., Tang, C.A., Liang, Z.Z., Ma, T.H. and Zhang, Y.B. (2009a), "Numerical simulation on water inrush process due to activation of collapse columns in coal seam floor", *J. Min. Safe Eng.*, **2**, 158-162.

Li, Q.F., Wang, W.J., Zhu, C.Q. and Peng, W.Q. (2009b), "Analysis of fault water-inrush mechanism based on the principle of water-resistant key strata", *J. Min. Safe Eng.*, **1**, 87-90.

Li, L.P., Li, S.C. and Zhang, Q.S. (2010a), "Study of mechanism of water inrush induced by hydraulic fracturing in karst tunnels", *Rock. Soil Mech.*, **2**, 523-528.

Li, S.C., Li, S.C., Zhang, Q.S., Xue, Y.G., Liu, B., Su, M.X., Wang, Z.C. and Wang, S.G. (2010b), "Predicting geological hazards during tunnel construction", *Rock Mech. Geotech. Eng.*, **2**(3), 232-242.

Li, S.C., Zhou, Z.Q., Li, L.P., Xu, Z.H., Zhang, Q.Q. and Shi, S.S. (2013), "Risk assessment of water inrush in karst tunnels based on attribute synthetic evaluation system", *Tunn. Undergr. Sp. Tech.*, **38**, 50-58.

Li, S.C., Xu, Z.H. and Ma, G.W. (2014), "A graph-theoretic pipe network method for water flow simulation in discrete fracture networks: GPNM", *Tunn. Undergr. Sp. Tech.*, **42**, 247-263.

Li, L.P., Lei, T., Li, S.C., Xu, Z.H., Xue, Y.G. and Shi, S.S. (2015a), "Dynamic risk assessment of water inrush in tunnelling and software development", *Geomech. Eng., Int. J.*, **9**(1), 57-81.

Li, L.P., Lei, T., Li, S.C., Zhang, Q.Q., Xu, Z.H., Shi, S.S. and Zhou, Z.Q. (2015b), "Risk assessment of water inrush in karst tunnels and soft development", *Arab. J. Geosci.*, **8**(4), 1843-1854.

Liao, W., Zhou, R.Y. and Li, S.Q. (2006), "Study on the non-linear forecast methods for water inrush from coal floor based on wavelet neural network", *China Safe Sci. J.*, **11**, 24-28.

Ling, S.X., Ren, Y., Wu, X.Y., Zhao, S.Y. and Qin, L.M. (2015), "Study on reservoir and water inrush characteristic in Nibashan Tunnel, Sichuan Province, China", *Eng. Geol. Soc. Territ.*, **6**, 577-582.

Liu, H.L., Yang, T.H., Yu, Q.L., Chen, S.K. and Wei, C.H. (2010), "Numerical analysis on the process of water inrush from the floor of seam 12 in Fangezhuang coal mine", *Coal Geol. Explor.*, **38**(3), 27-31.

Liu, Z., Jin, D. and Liu, Q. (2011), "Prediction of water inrush through coal floors based on data mining classification technique", *Procedia Earth. Planet Sci.*, **3**, 166-174.

Ma, L., Liu, Y. and Zhou, X.P. (2010), "Fuzzy comprehensive evaluation method of F statistics weighting in identifying mine water inrush source", *Int. J. Eng. Sci. Tech.*, **2**(7), 123-128.

Marinelli, F. and Niccoli, W.L. (2000), "Simple analytical equations for estimating ground water inflow to a mine pit", *Groundwater*, **38**(2), 311-314.

Meng, Z.P., Li, G.Q. and Xie, X.T. (2012), "A geological assessment method of floor water inrush risk and

its application", *Eng. Geol.*, **143**, 51-60.

Qian, Q.H. (2012), "Challenges faced by underground projects construction safety and countermeasures", *J. Rock Mech. Eng.*, **31**(10), 1945-1956.

Qian, Q.H., Li. Z.P. and Fu, D.M. (2002), "The present and prospect of application of tunnels in China's underground engineering", *J. Undergr. Sp.*, **22**(1), 1-11.

Qu, H.F., Liu, Z.G. and Zhu, H.H. (2006), "Technique of synthetic geologic prediction ahead in tunnel informational construction", *Chinese J. Rock Mech. Eng.*, **25**(6), 1246-1251.

Shang, Y.J., Yang, Z.F., Zeng, Q.L., Sun, Y.C., Shi, Y.Y. and Yuan, G.X. (2007), "Retrospective analysis of TBM accidents from its poor flexibility to complicated geological conditions", *J. Rock Mech. Eng.*, **26**(12), 2404-2411.

Shi, L.Q. and Singh, R.N. (2001), "Study of mine water inrush from the tunnel floor strata through faults", *Min. Water. Environ.*, **20**(3), 140-147.

Shi, L. and Xu, L.Y. (2010), "Prediction of mine water inrush sources based on cluster analysis of hydro geochemical features", *Coal Sci. Tech.*, **3**, 97-100.

Shi, L.Q., Qiu, M., Wei, W.X., Xu, D.J. and Han, J. (2014), "Water inrush evaluation of coal seam floor by integrating the water inrush coefficient and the information of water abundance", *Int. J. Min. Sci. Tech.*, **24**(5), 677-681.

Wang, J.H. and Lu, C.C. (2007), "A semi-analytical method for analyzing the tunnel water inflow", *Tunn. Undergr. Sp. Tech.*, **22**(1), 39-46.

Wang, J.T. and Wang, X.L. (2011), "Discussion on water inrush coefficient method applied to predict water inrush danger of seam floor based on Gaojiata Mine as example", *Coal Sci. Tech.*, **7**, 106-111.

Wang, L.G., Song, Y. and Miao, X.X. (2003), "Study on prediction of water-inrush from coal floor based on cusp catastrophic model", *Chinese J. Rock Mech. Eng.*, **22**(4), 573-577.

Wang, T.T., Wang, W.L. and Lin, M.L. (2004), "Harnessing the catastrophic inrush of water into new Yungchuen Tunnel in Taiwan", *Tunn. Undergr. Sp. Tech.*, **19**(4-5), 418-426.

Wang, J.S., Wang, L., Cao, Z.G., Liu, Z.G., Wang, L. and Zhu, H. (2007), "Practice on synthetic geological prediction ahead of construction of Xiamen subsea tunnel", *Chinese J. Rock Mech. Eng.*, **26**(11), 2309-2317.

Wang, Y., Yang, W., Li, M. and Liu, X. (2012), "Risk assessment of floor water inrush in coal mines based on secondary fuzzy comprehensive evaluation", *Int. J. Rock Mech. Min. Sci.*, **52**, 50-55.

Wu, Q., Xu, H. and Pang, W. (2008), "GIS and ANN coupling model: an innovative approach to evaluate vulnerability of karst water inrush in coalmines of north China", *Environ. Geol.*, **54**(5), 937-943.

Wu, Q., Liu, Y., Liu, D. and Zhou, W. (2011a), "Prediction of floor water inrush: the application of GIS-based AHP vulnerable index method to Donghuantuo coal mine, China", *Rock Mech. Rock Eng.*, **44**(5), 591-600.

Wu, Q., Zhu, B. and Liu, S.Q. (2011b), "Flow-solid coupling simulation method analysis and time identification of lagging water-inrush near mine fault belt", *Chinese J. Rock Mech. Eng.*, **30**(1), 93-105.

Xu, J.L., Zhu, W.B. and Wang, X.Z. (2011), "Study on water-inrush mechanism and prevention during coal mining under unconsolidated confined aquifer", *J. Min. Safe. Eng.*, **3**, 333-339.

Xu, Z.H., Ma, G.W. and Li, S.C. (2014), "A Graph-theoretic Pipe Network Method for water flow simulation in a porous medium: GPNM", *Int. J. Heat Fluid Fl.*, **45**, 81-97.

Yao, B.H., Bai, H.B. and Zhang, B.Y. (2012), "Numerical simulation on the risk of roof water inrush in Wuyang Coal Mine", *Int. J. Min. Sci. Tech.*, **22**(2), 273-277.

Yang, X.L. and Yan, R.M. (2015), "Collapse mechanism for deep tunnel subjected to seepage force in layered soils", *Geomech. Eng., Int. J.*, **8**(5), 741-756.

Yin, S.X. and Wu, Q. (2004), "Simulation and mechanism analysis of water inrush from karst collapse columns in coal floor", *Chinese J. Rock Mech. Eng.*, **15**, 2551-2256.

Zarei, H.R., Uromeily, A. and Sharifzadeh, M. (2012), "Identifying geological hazards related to tunneling in carbonate karstic rocks - Zagros, Iran", *Arba. J. Geosci.*, **5**(3), 457-464.

Zhang, J.C. (2005), "Investigations of water inrushes from aquifers under coal seams", *Int. J. Rock Mech. Min. Sci.*, **42**(3), 350-360.

Zhang, J.J. and Fu, B.J. (2007), "Advances in tunnel boring machine application in China", *J. Rock Mech. Eng.*, **26**(2), 226-238.

Zhang, J. and Peng, S. (2005), "Water inrush and environmental impact of shallow seam mining", *Environ. geol.*, **48**(8), 1068-1076.

Zhang, H.S., Xue, G.W., Shi, X.W., Liu, H.F. and Hu, Y.Q. (2009), "Prediction of water inrush from coal seam floor confined based on geo-information composite overlay analysis", *J. China Coal Soc.*, **34**(8), 1100-1104.

Zhou, Z.Q., Li, S.C., Li, L.P., Shi, S.S. and Xu, Z.H. (2015), "An optimal classification method for risk assessment of water inrush in karst tunnels based on the grey system", *Geomech. Eng., Int. J.*, **8**(5), 631-647.

Zhu, W.C. and Wei, C.H. (2011), "Numerical simulation on mining-induced water inrushes related to geologic structures using a damage-based hydro mechanical model", *Environ. Earth Sci.*, **62**(1), 43-54.

Zhu, Q.H., Feng, M.M. and Mao, X.B. (2008), "Numerical analysis of water inrush from working-face floor during mining", *J. China U. Min. Tech.*, **18**(2), 159-163.

*CC*